Preparation and characterization of colloidal crystals

Research work presented by
Da. María Yoldi Sangüesa
10th March 2005

Department of Physics
and Applied Mathematics
School of Science
University of Navarra

Universidad de Navarra, E-31080 Pamplona, Navarra (Spain)

Servicio de Publicaciones de la Universidad de Navarra

ISBN 84-8081-076-9

Preparation and characterization of colloidal crystals

Research work presented by
Da. María Yoldi Sangüesa
10th March 2005

Department of Physics
and Applied Mathematics
School of Science
University of Navarra

Universidad de Navarra, E-31080 Pamplona, Navarra (Spain)

Dr. Wenceslao González Viñas y Dr. Rafael Sirera Bejarano, profesores de la Facultad de Ciencias de la Universidad de Navarra,

CERTIFICAN: que la presente Memoria, ***"Preparación y caracterización de cristales coloidales"*** ha sido realizada bajo nuestra dirección en la **Facultad de Ciencias de la Universidad de Navarra** y en el **Fraunhofer Institut für Angewandte Polymerforchung (IAP, Gölm, Alemania)** por Dña. María Yoldi Sangüesa.

Para que conste, se firma la presente certificación en Pamplona, el diez de marzo de dos mil cinco.

Fdo. Wenceslao González Viñas

Fdo. Rafael Sirera Bejarano

Acknowledgements

First of all, I would like to acknowledge to my supervisors, Dr. González–Viñas and Dr. Sirera, not only for introducing me in the interesting world of photonics, but also for their patience and their strong support in the difficult situations.

Then, I acknowledge to the members from the Physics and Applied Mathematics Department of the University of Navarra for their interest and their advices: Sergio Ardanza, Pilar Ayúcar, Stefano Boccaleti, Jean Bragard, Javier Burguete, María Jesús Chasco, Emilio Díaz, Pedro Elizalde, Jorge Elorza, Ángel Garcimartín, Héctor Mancini, Diego Maza, Carmen Palacios, Antonio Peláez, Carlos Pérez and Fernando Varela. And to my partners in the Department for their help and for all the unforgettable moments that we have enjoyed together: Cristina Arcos, Roberto Arévalo, Angela Bernardini, Sergio Casado, Paulina Cuello, Alberto De la Torre, Joaquín Goñi, Santiago Madruga, Manu Mancini, Cristian Mankoc, Carolina Mendoza, Montserrat Miranda, Martín Pastor, Begoña Peña, Fernando Perales, Cecilia Wolluschek e Iker Zuriguel.

I would also like to acknowledge to Dr. Görnitz and his collaborators, Dr. Paulke, Dr. Wagner, Dr. Goldenberg and Dr. Stumpe, for their kindness and their supervision during my stay in the Fraunhofer Institut für Angewandte Polymerforchung (IAP), in Gölm (Germany). And to my parners in the IAP: Flavie, Martin, Rainer, Robert, Udom and Stephan for the "17^{00} Stunde Kaffee". And thank you to Kasy. Berlin would have not been the same without you.

Thank you to my best friends, Arrate, Itziar, Nerea y Zaida, for being an unconditional support for more than 20 years. You are "monería". Thanks also to Eva and Nekane for being always by my side. If having a friend is having a treasure, I will be the richest person in the world.

Now I would like to remind Abel, for giving me back the illusion, the happiness and the confidence. I know that it is no possible to thank you enough, but I would try: THANK YOU.

I acknowledge specially to my parents and my brother David. You have taught me the most important lessons and you have always found the proper words to encourage me in the hard moments. Thank you!

Finally, I acknowledge to the Spanish MECD for the AP2002-2000 scholarship, which also supports me to do the 6 months stay in the IAP.

This work was partly supported by the Spanish MCyT (projects BFM2002-02011, MAT2003-02369) and PIUNA2003-34.

Contents

List of Figures

Preface

Electronics, the technology of electrons, has meant a huge revolution in the field of communications and computing in the last century. Although electronics is to be further pursued, the limit of miniaturization is being reached for the processing and storage of information. In order to continue in the development of information society, nowadays other kind of technology is required. Photonics, the technology of photons, seems to be a different way to satisfy these demands. Since the photon is much more efficient than the electron in the transmission, processing and storage of information, the miniaturization of the devices will not be a problem no longer.

Two different approaches to a common problem were published, simultaneously but also independently, by Yablonovitch [1] and John [2] in 1987. Both agreed that the photon was the best choice of source and channel of the information carrier, but Yablonovitch focussed on the development of further materials in order to take the most of benefits of spontaneous emission inhibition; while John suggested some materials which, due to their refractive index (n), could allow to study the strong inhibition of light transmission.

Since the invention of laser, lots of other photonic elements have been widely developed. However, there is still a long way to go in this field. On one hand, most of the concepts relating to electronics are explained in solid-state concepts and the explanations in photonics are returning to the source (i.e. Bloch Theorem). On the other hand, although the theoretical concepts are well-known, technological aspects of the problem have to be studied. There are two approaches which are mainly unknown: the three-dimensional structures and the fabrication methods different to those adopted to microelectronics, which lead to two-dimensional structures.

Photonic crystals (PCs) are a type of materials which present ordered structures in two different scales. First, they could be microscopically structured in the atomic range. They are also structured in the scale of the light wavelength (mesoscale). From these two different scales arise new phenomena, like the inhibition of light propagation.

Based on the theories of self–assembly, colloidal systems are being used as a cheap and natural starting point for the fabrication of PCs. The scientific community has a lot to do in this field, because none PC has been prepared by this methodology yet.

The aims of this study were the preparation and the characterization of optical materials based on three dimensional ordered arrays of colloidal latex particles, which are also called colloidal crystals (CCs). Although these multilayered latex particles arrays do not exhibit a photonic bandgap (PBG), the fabrication and the

research of the optical properties of CCs based on polymeric colloidal particles are not only useful as templates to synthesize PCs but also because, due to their composition and their structure, they could present very interesting applications, such as those derived of the interaction with light (diffraction, interference, scattering, absorption, inhibition, ...), maximal packing density, maximal structural stability, maximal catalytic and reactivity inside them and the ability to create media for information storage (pre–formatted substrates), among others.

Lots of different techniques and sources of knowledge contribute to develop and explain the photonic phenomena. Physicists, chemists and engineers work together in the photonic field. This interdisciplinary nature of the problem enriches it.

The main ideas of polymerization and colloidal crystallization are commented in the Introduction. In chapter 1, not only modified emulsion and dispersion polymerization techniques based in styrene and acrylate monomers, but also the surface functionalization and the purification and characterization of the colloidal latex particles synthesized are explained in detail. In chapter 2, the fabrication of 3D ordered arrays of colloidal particles by vertical deposition and sedimentation methods, and the investigation of the optical properties and crystalline structure of the colloidal crystals by spectroscopy, optical microscopy and optical diffraction techniques are explained. Finally, the conclusions of the study are reported in the last chapter.

The main aims of this work are:

1. Synthesis of highly monodisperse polystyrene particles in the range of 1 μm
2. Surface functionalization in order to enhance self-assembly
3. Cleaning and purification of the latexes
4. Determination of the main characteristics of the particles, such as its concentration, surface charge density and electrophoretic mobility, size and polydispersity
5. Study of the main parameters which take part in the process of self-assembly
6. Optimize these parameters in order to minimize the number of defects in the final structures, improving the quality of the colloidal crystals prepared
7. Determination of the crystalline structure and the optical properties of the colloidal crystals prepared

Although this study was developed mostly in the Fraunhofer Institut für Angewandte Polymerforchung (IAP, Gölm, Germany), some of the stages have also been done in the Department of Physics and Applied Mathematics of the University of Navarra (UNAV) A scheme of the methodology of our study is shown in figure 1.

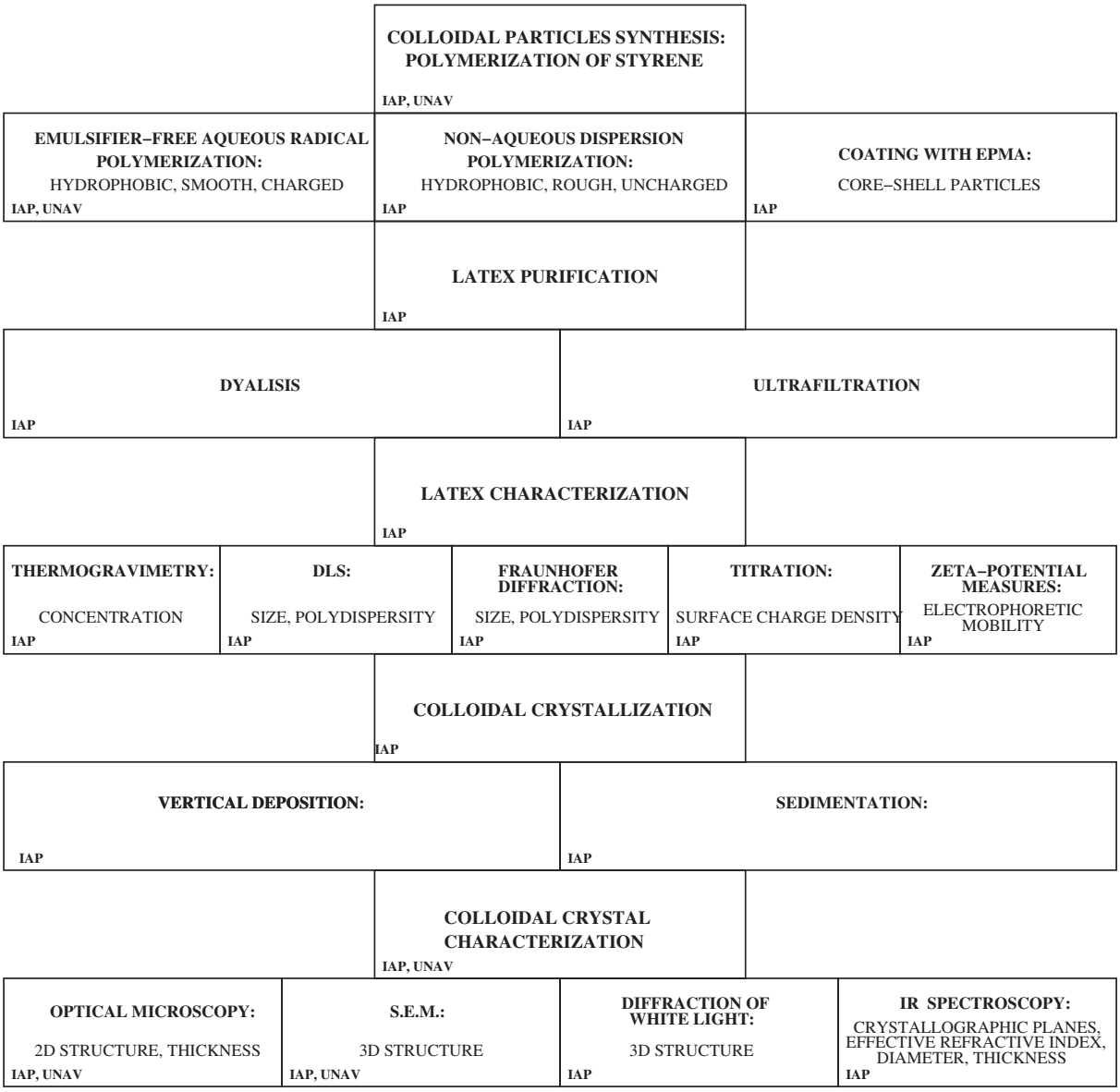

Figure 1: Scheme of the stages of the study

Introduction

Preparation and characterization of colloidal particles

Colloidal comes from the Greek word $\kappa o\lambda\lambda\alpha$, and means "glue–like". An element or compound is considered colloidal when particles are sized between 5 nm and 10 μm, and the energy of the substance is predominantly governed by surface effects [3; 4; 5].

Colloidal particles (silica, alumina, titanium oxide, polystyrene, polymethacrylat, among others) can be prepared by **sol–gel** [6] or **polymeric methods**.

In this study, we have worked with polymeric colloidal particles, synthesized by different techniques of emulsion and dispersion based on polymerization of styrene and acrylate monomers

Polymers are large molecules made up of simple repeating units [7; 8]. The name is derived from the Greek $\pi o\lambda\upsilon$, meaning "many", and $\mu\epsilon\rho o\sigma$, meaning "part". If only a few units (4–20) are joined together, the resulting compound is called an *olygomer* ("few parts"). Polymers are synthesized from simple molecules called *monomers* by a process called *polymerization*.

A polymer prepared from a single monomer is called *homopolymer*. If two or more monomers are employed, the product is a *copolymer*, which is called *random*, *alternating* or *block copolymer*, if the monomeric units are distributed randomly, in alternating fashion or in blocks, respectively.

There are two types of monomers: olefines and functionalized monomers. The first ones have no reactive functional groups, while the second ones present at least two of them.

End groups are the structural units that terminate the polymer chains, also called *backbones*. *Degree of polymerization (DP)* refers to the total number of structural units, including end groups. It is related to both chain length and molecular weight. Because polymer chains within a given polymer sample are almost always of varying lengths, the *average degree of polymerization* ($\bar{DP}$) is mainly used.

There are four different definitions of molecular weight related to polymers, which are determined by different techniques:

1. Number average molecular weight ($\bar{M}_n$)

$$\bar{M}_n = \frac{\sum_i N_i M_i}{\sum_i N_i} = \frac{\sum_i w_i}{\sum_i \frac{w_i}{M_i}} \tag{1}$$

where N_i represents the number of particles, and M_i and w_i are the molecular weight and the weight of the particle i, respectively.

$\bar{M}_n$ is determined by membrane osmometry, end–group titration, mass spectrometry, refractive index measurements and colligative properties (cryoscopy, ebullioscopy and vapor pressure osmometry).

2. Weight average molecular weight ($\bar{M}_w$)

$$\bar{M}_w = \frac{\sum_i N_i M_i^2}{\sum_i N_i M_i} = \frac{\sum_i w_i M_i}{\sum_i w_i} \tag{2}$$

$\bar{M}_w$ is determined by light scattering, Small Single Neutron Scattering (SANS) and sedimentation velocity (ultracentrifugation).

3. Viscous average molecular weight ($\bar{M}_v$)

$$\bar{M}_v = \left[\frac{\sum_i N_i M_i^{1+a}}{\sum_i N_i M_i} \right]^{\frac{1}{a}} \tag{3}$$

where a is the parameter of the viscosimetric equation of Mark-Houwink [9]

$\bar{M}_v$ is determined by intrinsic viscometry.

4. Z average molecular weight ($\bar{M}_z$)

$$\bar{M}_z = \frac{\sum_i N_i M_i^3}{\sum_i N_i M_i^2} = \frac{\sum_i w_i M_i^2}{\sum_i w_i M_i} \tag{4}$$

$\bar{M}_z$ is determined by gel permeation chromatography (GPC), fractional solution, fractional precipitation and thin–layer chromatography (TLC).

Polydispersity index (PI) is the ratio between $\bar{M}_w$ and $\bar{M}_n$, and it is used as an indication of the width of the molecular weight range in a polymer sample. The

system having a range of molecular weights is called *polydisperse*. If all polymer molecules present the same molecular weight, the system is *monodisperse*.

$$PI = \frac{\bar{M}_w}{\bar{M}_n} \tag{5}$$

The **traditional classification** for polymers was first proposed by Carothers [10] and it is based on whether the repeating unit of the polymer contains the same atoms as the monomer. An *addition polymer* has the same atoms as the monomer in its repeating unit, whereas *condensation polymer* contain fewer because of the formation of byproducts during the polymerization process. The corresponding polymerization processes are the called addition and condensation polymerization [11].

Addition polymerization involves the breaking of double or triple bonds, which are used to link monomers into chains. The process can be divided in three stages: initiation, propagation and termination. The molecule which start the process is called initiator and defines the specific type of addition mechanisms. It is distinguished radically, ionic or coordination polymerization, when the initiator is a radical, an ion (cation or anion) or a Ziegler–Natta catalyst (halogenure of titanium or vanadium), respectively.

Condensation polymerization requires functionalized monomers, which can react ones to others. Each monomer should be at least double functionalized. These reactions can be achieved typically through reacting molecules incorporating alcohol, amine or carboxylic acid functional groups. These monomers bond together through condensation reactions. A condensation reaction, also known as a dehydration reaction, is a chemical reaction in which two molecules react each other with the concurrent loss of water or ammonia.

The condensation reaction proceeds in two steps: a nucleophilic addition and an elimination.

Labelling a given polymer as the addition or condensation type is complicated. To avoid ambiguity, the reactions of polymerization are nowadays more commonly characterized according to the **polymerization mechanism**. In chain-growth polymerization, the molecular weight increases by the successive linking of monomer molecules to the end of a growing chain. In step growth polymerization, the polymer chains are built up in a stepwise fashion by the random union of monomer molecules to form dimers, trimers, and higher species throughout the monomer matrix. Most *chain–growth polymers* are addition polymers, and most *step–growth polymers* are condensation ones.

There are different **methods of polymerization**. *Bulk polymerization* involves only the monomer and a monomer–soluble initiator (in addition) or the monomer/monomers and catalysts (in condensation). In *solution polymerization*, the monomer and the initiator are dissolved in a solvent, which lowers the viscosity, assisting heat transfer and reducing the likelihood of auto–acceleration. In *suspension polymerization*, the monomer is dispersed in small droplets, which are suspended in an inert medium (water in most of the cases), which absorbs the heat generated during the polymerization. As the initiator is solved in the monomer droplets, the reaction takes place inside them. And in *emulsion polymerization*, the monomer is

dispersed in an aqueous phase with an emulsifier. The emulsifier generates micelles, which also contain monomer. As the initiator is not soluble in the monomer but soluble only in the aqueous dispersion medium, the polymerization takes place inside the micelles and the monomer droplets are mainly storages of monomers. After the polymerization, the emulsifier should be removed by cleaning the polymer.

After synthesis, polymers should be carefully purify. This is very important not only for analytical characterization, but also because their mechanical, electrical and optical properties are strongly influenced by impurities. Besides, even traces of impurities may cause or accelerate degradation or crosslinking reactions [8]. The conventional techniques for the purification of low molecular weight compounds, such as sublimation and crystallization, are not applicable to polymers. The most used **methods of purification** of polymers are *distillation*, *dialysis* (separation of low molecular weight components from water–soluble components), *ultrafiltration* (also called electrodialysis) and *serum replacement* (precipitate the polymer and re–dissolve it in another solvent, where the impurities are not soluble) .

Colloidal crystallization

A *Colloidal dispersion* is a two–phase system in which the kinetic units, called *colloidal particles*, that are dispersed through the solvent are much larger in size than the molecules of the solvent. The finely divided colloidal particles are called the disperse phase, and the bulk substance is named the dispersion medium. If the dispersion medium is water, the colloidal dispersion is called *latex*.

Freundlich[12] classified the colloidal dispersions in two groups, called *lyophilic* (solvent loving) and *lyophobic* (solvent hating), depending on the possibility of the system of being redispersed if it was dry out. Because of that, Kruyt[13] proposed to label the systems as reversible (lyophilic) and irreversible (lyophobic). One contributing factor to the different behavior between reversible and irreversible systems is the way in which the dispersion medium is able to interact with the dispersed particles.

The lyophilic colloid solution is thermodynamically stable because there is a reduction in the Gibbs free energy when the solute is dispersed ($\Delta G<0$). The strong interaction between solute and solvent supplies enough energy to break up the disperse phase ($\Delta H<0$) and any reduction in solvent entropy due to the interaction with solute is compensated by the entropy increase of the solute ($\Delta S>0$).

For the lyophilic colloid, the Gibbs free energy increases ($\Delta G>0$) when the dispersed phase is distributed through the dispersion medium so that it is a minimum when the dispersed phase remains in the form of a single big particle. A lyophilic colloid can only be dispersed if its surface is treated in some way that causes a strong repulsion between particles. Although these kind of colloidal dispersions are thermodynamically unstable, there are several methods to prevent particles from aggregating for long periods[14].

While the DLVO theory, which is explained in chapter 1, describes properly the interaction between particles of a lyophobic colloid, the behavior of lyophilic

colloids is more difficult to describe, due to strong solvent effects. Because of that, the systems we are going to study are the lyophobic (irreversible) ones.

As it has been told, a colloidal system consists of a large number of individual particles dispersed in a continuous medium. Since the particles are under Brownian motion, they are continually colliding themselves and remain as individual particles only if any mechanism prevents aggregation during a collision. There are two ways in which that can be done:

1. Electrostatic stabilization

   Particles are given an electric charge (either positive or negative). Because of that, they repel strongly each other.

2. Steric stabilization

   Particles are coated with an adsorbed layer of some material, which is itself who prevents the close approach of the colloidal particles.

A system is colloidally unstable if the collisions result in the formations of aggregates. The aggregation process is called *coagulation*, when particles come in close contact as a result of changes in the electrical double layer around them (see chapter 1), and *flocculation*, when particles are linked together by a polymer.

Coagulation can be studied both at a microscopic and at a macroscopic level. At a microscopic level we follow the individual collisions between pairs of particles, to determine the rate of formation of doublets, triplets, ... This behavior is related to the diffusive motion of particles and the forces between them.

If coagulation continues, the particle aggregates became large enough to be macroscopically visible and are named *flocs*. If their density is higher than the dispersion medium, settle quite quickly from it leaving a more or less clear supernatant. However, if floc density is lower than the surrounding medium, the aggregate accumulates at the top by a process called *creaming*.

Uniform colloidal microspheres dispersed in a fluid medium have a natural tendency to organize themselves into regular three–dimensional arrays. The mechanism responsible for this phenomena is called *colloidal self–assembly*, and offers means of distributing colloidal particles in complex three–dimensional structures with order extending, in principle, over macroscopic dimensions.

If the colloidal particles are charged, every colloidal particle is covered by several contra–ion layers of alternating positive–negative charge, called the "Stern double layer" (see chapter 1). The screening length of Debye–Hückel is defined as the distance where the influence of the particle charge is neutralized.

Derjaguin and Landau in 1941, and Verwey and Overbeeck in 1945 proposed a theory, called DLVO theory, to explain the behavior of this double layer. The partition function for N simple ions of charge q_i arrayed at positions $\vec{r}_i$ in the static potential $\phi(\vec{r})$ is

$$Q = Q_0 \int_\Omega (d\vec{r}_1 ... d\vec{r}_N)\, e^{-\frac{V(\vec{r}_i)}{k_B T}} \tag{6}$$

where

$$V(\vec{r}_i) = \frac{1}{\epsilon} \sum_{i=1}^{N} q_i \phi(\vec{r}_i) \tag{7}$$

is the total Coulomb energy, the pre–factor Q_0 results from integrals over momenta and $k_B T$ is the thermal energy at temperature T. All charged species in the system, including the aggregates (macroions), contribute to $\phi(\vec{r})$.

Finally, if the colloidal particles are charged and an electric field is applied to the dispersion, new forces should be taken into account. On one side, the electrical repulsion between the particles and on the other side, the electrical interaction with the electrodes. These electric forces are coupled to the hydrodynamic fields. Because of that, electrohydrodynamic is needed to make a "full description".

If the electrical field reinforces the gravitational one, the process consists of a natural sedimentation forced by electric fields and it is called electrophoresis.

As an analogy to the well–known ordered structures of atoms, two general types of structures could be distinguished: *colloidal crystal* and *colloidal glass*. The first one presents a long range order, while the second one does not.

These structures show interesting properties, such as:

1. Special optical properties. When the mesoscopic characteristic length is of the order of the light wavelength, dispersion is more important than absorption.

2. Large ratio area/volumen. Because of that, surface effects are most important in these systems.

Brief revision

Several techniques of self–assembly have been proposed to prepare colloidal crystals. Gravitational sedimentation [15; 16; 17] or sedimentation forced by different agents as electrostatic immobilization [18], colloidal crystal templating [19], vertical deposition [20; 21; 22], shear alignment [23], oscillatory shear [24] or flow assisted electrophoresis [25] are some examples. All of them are based on the idea that, under the proper conditions, colloidal particles assembly spontaneously into ordered structures.

The mechanism of vertical deposition consists on several steps. In principle, when colloidal particles are partly immersed in a thin layer of liquid, lateral capillary forces cause an attractive interaction between them, then the particles are pushed together and nucleate forming an hexagonal close–packing ordered monolayer. On the other hand, surface stabilization (colloidal stability) of the particles is important to prevent uncontrolled aggregation in the early stage of self–assembly. Flow of solvent brings in more spheres and the monolayer grows. The mechanism to explain the formation of three–dimensionally ordered structures is more complicated, and the forces of surface tension in the meniscus region are responsible to close–packing the spheres, consolidating them into an ordered crystal. So, this phenomena is not as simple as it seems to be and, in order to understand it better, it is useful to attend how it works in nature.

Natural gemstone opals have been structurally and optically investigated by Sanders et al [26; 27]. They consist of layers of hexagonally packed silica particles, which are adhered by van der Waals' forces and, perhaps, by cementation around the contacts (preferential precipitation of dissolved minerals at the contact points). In a natural opal, the close–packed layers stack to form a three dimensional solid. Three different stackings should be considered: ABCABC... (face centered cubic, fcc), ABABAB... (hexagonal close–packing, hcp) or ABCAB... (random hexagonally close–packing, rhcp) structures. Natural opals have shown to be rhcp [26; 27], structure with limited use as a photonic crystal. Theory predicts that for a colloidal crystal of hard spheres the fcc structure is the energetically most stable [28; 29; 30]. However, the difference between fcc and hcp energy is extremely small ($<10^{-3}K_BT$ per particle). If static self–assembly, process driven by thermodynamic equilibrium, takes place it can observed either a fcc or a mixture of fcc and hcp (rhcp), depending on the conditions.

In contrast, sedimented synthetic opals exhibit structures that are fcc, but with 10-20% of stacking faults [31]. Therefore, sedimented opals have a preference for fcc packing. As planar opals are formed within a few hours, they are unlikely to have time enough to find the equilibrium state by thermal fluctuations. Convective assembly hypothesis [32], based on the important role which plays the solvent flow through the interstitial sites of the close–packed spheres during the opal growth, justifies the strong preference of planar synthetic opals to the fcc structure.

Unsolved questions

Regarding to the colloidal crystallization, the most important research fronts are:

1. Improving the crystal quality in order to avoid undesired defects

   The band structure, the cPBG (complete Photonic Band Gap) and the other properties of photonic crystals requires an structure with infinite periodicity in refractive index. Because of that, structures with big number of defects are not usable for technologic applications.

2. The introduction of controlled defects

   Having a better control of the process will allow to introduce controlled defects. This is very interesting in order to create structures with interesting potential technological applications such as guides or resonant cavities.

Chapter 1

Preparation and characterization of colloidal particles

1.1 Polymerization

There are several methods to prepare hydrophobic polystyrene (PS) latex particles with a narrow size distribution and a diameter in the order of 1μm.

Large, charged PS particles can be prepared via classical emulsion polymerization [33] and by an emulsifier–free, aqueous radical polymerization [34; 35]. The last one was selected due to its better reproducibility (latex BMG-7). These hydrophobic particles were electrostatically stabilized, but they were also coated with a hydrophilic shell to increase their stability by electrosterical interactions [36] (latex BMG-24).

On the other hand, large and uncharged PS (sterically stabilized tentacle) particles with 2.5μm diameter were also synthesized by non–aqueous dispersion polymerization [47; 36] (latex BMG-60).

A simple scheme of these types of polystyrene particles is shown in figure 1.1.

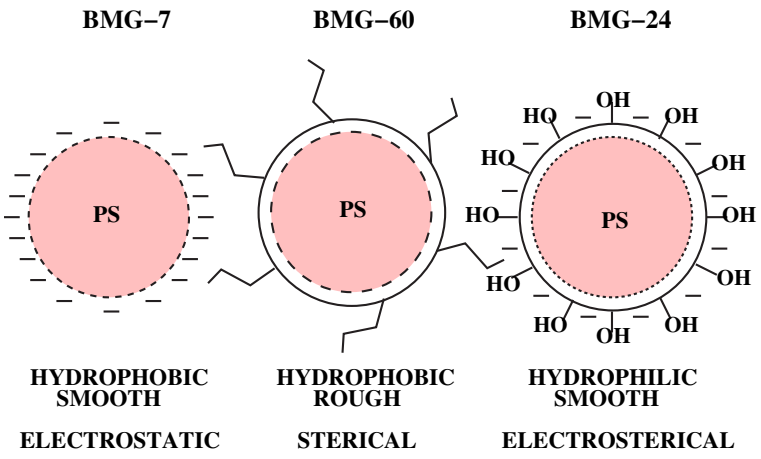

Figure 1.1: Scheme of the three different types of polystyrene particles synthesized in this work.

The styrene polymerization occurs through a mechanism of free radicals. Because of that, the anionic and cationic tails of the chains are quickly neutralized by the water. The starting step takes place when the initiator, such as $K_2S_2O_8$ in emulsifier–free aqueous radical polymerization and when core-shell particles are synthesized, or such as α-α'-azoisobutylnitrile (AIBN) in non–aqueous dispersion polymerization, generates a radical which reacts with a molecule of monomer. This way generates an active chain of polystyrene, which reacts with more molecules of styrene. This step, in which the polymer grows, is called propagation stage. The termination step takes place when the free radical is neutralized (see figures 1.2 and 1.3).

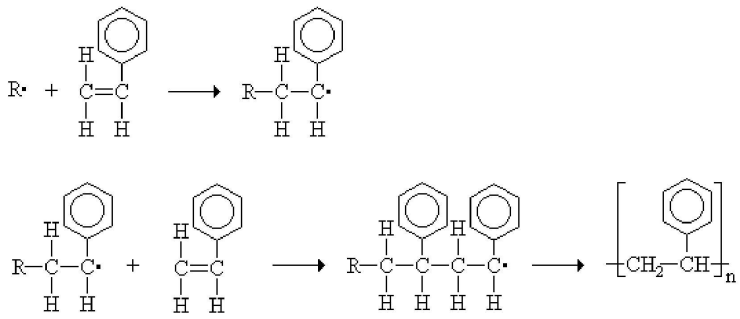

Figure 1.2: Polymerization of the styrene by a free radical mechanism.

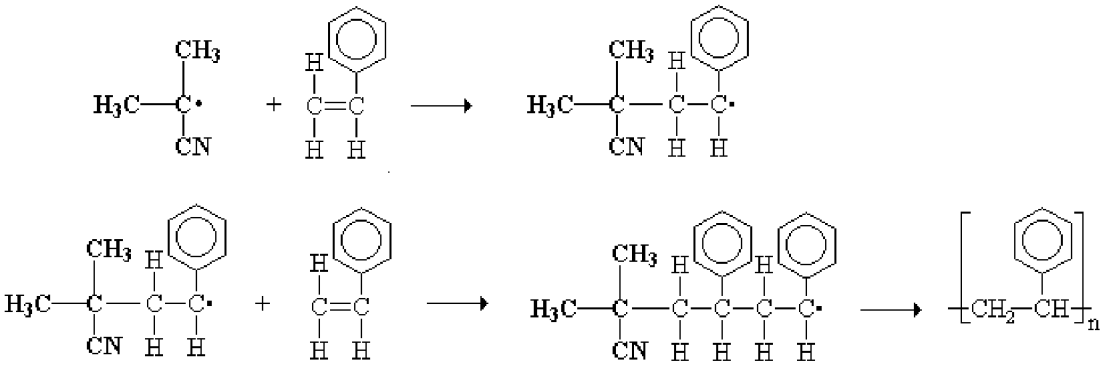

Figure 1.3: Polymerization of the styrene by a free radical mechanism, using AIBN as initiator.

1.1.1 Emulsifier-free, aqueous radical polymerization

This method of polymerization is called "solution polymerization", because both the monomer (styrene) and the initiator ($K_2S_2O_8$) are dissolved in a solvent (ultra–pure water), which lowers the viscosity, assisting heat transfer and reducing the likelihood of auto–acceleration. The electrolyte, used to control the ionic force of the media, is also dissolved in the same solvent.

Experimental section

1. Substrates and material
   Ultra pure water, 1 μS/cm conductivity, was used from a Mili-Q water system. Pure $K_2S_2O_8$, KH_2PO_4 and styrene are provided by Fluka laboratories.

2. Experimental system
   The samples were put in the reactor shown in figure 1.4.

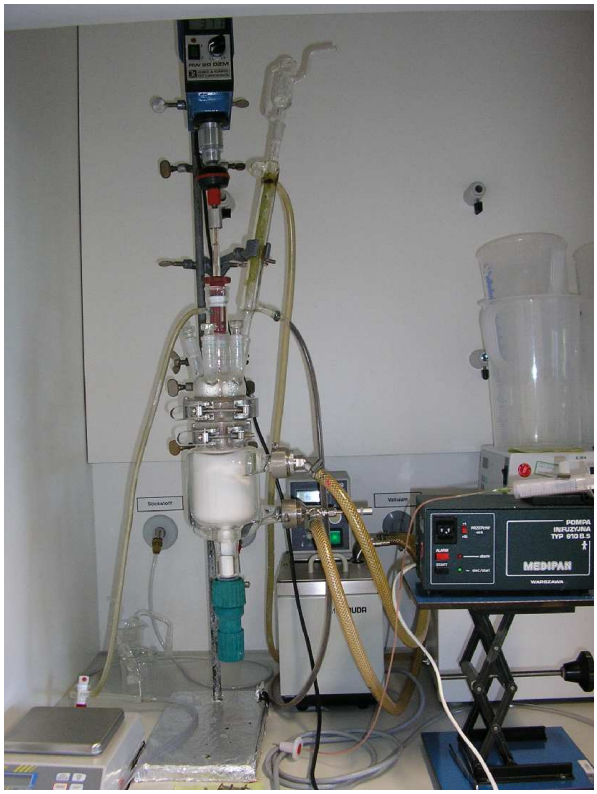

Figure 1.4: Reactor.

Method

The procedure was the following: 0.010 g of KH_2PO_4 (the electrolyte) were dissolved in 180 ml of ultra pure water and put into a glass reactor, which is placed inside a extractor hood. 18.1 g of styrene were added. 0.198 g of $K_2S_2O_8$ (the initiator) were diluted in 20 ml of ultra pure water and placed inside an addition–ampoule coupled to the system. The reactor is closed and N_2 flow is applied to obtain a non-reactive atmosphere. Also, a cold water flow is used to refrigerate the system. The stirrer is set at 360 rpm. 15 minutes were required to have the system stabilized. Then, the temperature is set at 60°C, afterwards to stabilize the system, 20 minutes should be waited. Finally, the initiator was added to the mixture, in order to start the polymerization, and 24 hour later, the mixture was taken out from the reactor to a plastic bottle. The reactor was cleaned with hot water.

This type of latex is denominated BMG–7. It consists on an aqueous dispersion of hydrophobic and smooth 1μm diameter particles, electrostatically stabilized. As these kind of particles present high number of negative charges on their surfaces, the latex is stable due to the electrostatic repulsion between the particles.

The advantages of this type of polymerization are:

1. all the monomer reacts
2. latex can be used without purification
3. can be controlled termically
4. materials with low T_g can be prepared
5. low viscosity

And the disadvantage

1. high sensibility to external conditions

1.1.2 Non–aqueous dispersion polymerization

This method of polymerization is another example of "solution polymerization". In this case, the solvent were all the monomer (styrene) and the initiator (AIBN) are dissolved is ethanol. It is also required a stabilizer (PVK–30) and a co-stabilizer (aerosol—OT) to keep the solution stable enough during the hole process of polymerization. They are also dissolved in ethanol.

Experimental section

1. Substrates and material
   Ultra pure water of 1 μS/cm conductivity, was used from a Mili-Q water system.
   All the reactive substances were provided by Fluka Laboratories. Pure PVK–30 (polyvinylpirrolidone) was used as stabilizer, pure aerosol–OT (sodium bis−ethylhexylsulphosuccinate) as co-stabilizer, pure AIBN (α-α'-azoisobutylnitrile) as initiator and pure styrene as the monomer. Absolute ethanol was used as solvent.

2. Experimental system
   The samples were put in the same reactor shown in figure 1.4.

Method

The following procedure was used: 3.9 g of PVK–30 and 1.12 g of aerosol–OT were weighted, and dissolved (together) in 185 ml of absolute ethanol. 28.6 g of styrene were weighted inside the extractor hood. 0.286 g of AIBN were weighted and dissolved in 25 ml of absolute ethanol. When the stabilizer and co-stabilizer were

dissolved, they were put inside reactor and the monomer was added. An addition–ampoule was coupled to the reactor and all the system was closed. The cooler water and the N_2 flow were applied and the speed of the stirrer was set at 111 rpm. 30 minutes should be waited at room temperature, in order to stabilize the system. Then, the system was warmed at 70°C, and other 30 minutes were waited. Finally the initiator was added through the addition ampoule. The polymerization started and after 24 h, the solvent (ethanol) is removed by centrifugation 20 minutes at room temperature and 14000 rpm. PS particles and solvent become two different phases, which can be separated. The particles are re–dispersed in ultra pure water and centrifugation is applied one more time. After the second centrifugation, PS particles and solvent are separated and particles are re–dispersed again. The final clean latex is obtained.

This type of latex is called BMG–60, and consists on an aqueous dispersion of hydrophobic and rough 2.5 μm diameter particles, sterically stabilized. This means that the lateral chains of PKV and AIBN present on particles surfaces stabilize the particles by sterical effects.

The advantages of non-aqueous dispersion polymerization are:

1. easy control of the temperature

2. high control of the molecular weight

And the disadvantages:

1. solvent must be removed

2. chain transference to the solvent

1.1.3 Preparing core-shell particles

These type of particles can be prepared in two steps: first, highly hydrophobic polystyrene particles are synthesized (by the procedure of BMG-7) and then, they are coated by a thin layer of an hydrophilic polymer, which prefers to polymerize over the polystyrene particles rather than create new particles itself (such as epoxymethilmethacrylat, EPMA).

Experimental section

1. Substrates and material
   Ultra pure water, 1 μS/cm conductivity, was used from a Mili–Q water system. Pure $K_2S_2O_8$, Borax, EPMA (Epoxypropylmethacrylat) and styrene are provided by Fluka laboratories.

2. Experimental system
   The samples were put in the same reactor shown in figure 1.4.

Method

The procedure was the following: 200 ml of latex 4% (8 g of PS) were prepared, diluting dialyzed BMG–7 with ultra pure water. 0.1 g of borax were dissolved into the latex. 0.1 g of $K_2S_2O_8$ (the initiator) were dissolved in 20 ml of ultra pure water. 1 g of EPMA was weighted inside the extractor hood. The latex with the borax was put inside the reactor and the EPMA solution was added. An addition ampoule was coupled to the reactor, the initiator was placed inside it and the system was perfectly closed. The low N_2 flow and the cooler water flow were applied, at room temperature and with the stirrer at 350 rpm. 20 minutes were waited, to let the system stabilized. Then, the system was warm up to 60°C inside the reactor, and then other 20 minutes were waited to have the system stabilized again. Finally, the initiator was added to the mixture through the addition ampoule. The polymerization took place during 5 h. Then, the mixture was taken out from the reactor to a plastic bottle, and the reactor was cleaned with hot water.

This type of latex is denominated BMG–24. It consists on an aqueous dispersion of hydrophilic and smooth 1μm diameter particles, both electrostatically and sterically stabilized. This electrosteric stabilization is a combination of charge contributions (from charges on the particles surface or on tentacles) and steric contributions (from water-soluble polymer chains or tentacles, coupled to the surface) to colloidal stability.

The advantage of core–shell particles is their higher stability. This anionic hydrophilic core–shell latex type includes a Coulomb and also a steric contribution to stability. The steric component comes, in this case, from the hydrophilic shell and the polymer chains inside this shell.

The disadvantage of coating is that, if the process is not completely successful, very different types of particles are present in the latex.

1.2 Cleaning and purification

As it was said in the introduction, polymeric colloidal particles should be carefully purify after their synthesis. This is necessary not only for their analytical characterization, but also because their mechanical, electrical and optical properties are strongly influenced by impurities.

From all the techniques available to purify polymeric colloidal particles, we have selected dialysis and ultrafiltration.

Dialysis

100 ml of latex are put into a Visking dialyzing tubing of 36/32 size pore and 27 mm of diameter, provided by Serva. They are placed into a big bottle with ultra pure water and the conductivity of this water is measured each day, until it reaches the value of 1 μS/cm, with a conductimeter 660 Metrohm Swiss Made. The water is changed everyday, after the measure.

Ultrafiltration

The selected filter was put into the ultra–filtration tube and 400 ml of latex were introduced in it. Three different types of filters, of 75 mm diameter and different pore sizes, were used. PC MB Nuclepore Track-Etch Membrane (1 uM) from Whatman, PC MB Nuclepore (0.5 uM) from Corning Costar Corporation and US Millipore from Millepore Corporation. The selection depends on the particle size and on the required grade of purification. The 0.5 uM filter was used for routine experiments. A IKAMAG REO (from Drehzahl Electronic) stirrer working at 700 rpm was coupled to the system, and the ultra–filtration process took place during 7 days at room temperature and 3 bar. The pressure was controlled by a KNF floods pump. After taking out the latex, the system was intensively cleaned by circulating 400 ml of hot ultra–pure water during 10 minutes.

1.3 Characterization of the colloidal particles

Introduction

Several parameters of the synthesized latex were determined, such as the concentration, the hydrodynamic diameter (particle size) and the polydispersity, the surface charge density and the electrophoretic mobility (zeta potential, ζ).

Concentration

The concentration (in % w/w) was determined by a thermogravimetric method: 1g of latex was weighted with a KERN 770 balance and dried into an oven from Heraeus Instruments, by heating it 2h at 85°C.

Size and polydispersity

The particle size is determined by optical microscopy, by Dynamic Light Scattering (DLS) and by Fraunhofer diffraction. DLS is used to characterize small particles, with diameters in the nanometer or micrometer range (20 nm to 1μm). Fraunhofer diffraction is used with large particles (500 nm to 2 mm).

Optical microscopy

One drop of latex, diluted in 3 o 4 ultra pure water drops, is put on a microscope slide and covered with a deck glass. The size and the polydispersity of the latex can be observed by optical microscopy using an Olympus BH2 microscope.

Dynamic Light Scattering (DLS)

The mode of interaction of light with matter depends on the electronic structure of the material. The absorption of light takes place when the energy of the incident

photon is equal to the difference in energy of two states in the system. The scattering of light (LS) occurs when the light, as an oscillating electric field, distorts the distribution of the charges in the system and they, as accelerated charges, emit radiation in the form of scattered light.

We consider two types of scattering:

1. Rayleigh. The diameter of the particle is smaller than the wavelength of the radiation in the media. In this case, every particle is a scattering center.

2. Debye. The diameter of the particle is bigger than the wavelength of the radiation in the media. In this case, every particle present several scattering centers and there are interferences.

The boundary between the Rayleigh and the Debye scattering is

$$\phi_c = \frac{1}{200}\lambda \tag{1.1}$$

In the case we study, we work with Debye scattering.

The response of a system to an external electric field is called polarization. It depends of both the applied electric field and the polarizability of the system, which is the ability of the charge distribution to be deformed by the external stimulus [38]. Light is scattered at angles other than the forward directions because of fluctuations in the polarizability of the medium.

The intensity of scattered light depends on the spatial arrangement of the scattering centers. Moreover, since the molecules are under Brownian motion, the instantaneous intensity of the scattered light varies with time. According to this, two types of experiments can be made:

1. Integrated Intensity Light Scattering (ILS)

   It is observed interference patterns of scattering light, by measuring the intensity as a function of angle.

$$\frac{Kc\left(1+cos^2\theta\right)}{\Delta R_\theta} = \frac{1}{\bar{M}_w P\left(\theta\right)} + 2A_2c + \ldots \tag{1.2}$$

   where K is the optical constant for the system, c is the particle concentration, θ is the angle, ΔR_θ is the Rayleigh ratio (a normalized intensity of scattering), $\bar{M}_w$ is the weight average molecular weight, $P\left(\theta\right)$ is the particle structure factor (which depends of its form) and A_2 and ... are the second and more virial coefficients.

   As it can be observed in equation 1.2, the information that can be obtained from the ILS experiments is the average molecular weight, the radius of gyration of the molecule and internal spatial arrangement of the scattering centers (from the particle structure factor), and the virial coefficients.

2. Dynamic Light Scattering (DLS)

   It is studied the fluctuations in scattering light as a function of time [39]. The intensity of scattered light which is reported at a certain angle is an average, but its instantaneous value changes due to fluctuations in the particle concentration caused by the Brownian motion. In fluids, the smaller the particles, the faster the diffusion. In this way, not only the average value of the intensity of scattering is a function of the particle size (related to $\bar{M}_w$), but also of time. The correlation function is used to study the temporal relationship between two variables. If it is studied the temporal relationship between one variable and itself, then it is called autocorrelation function.

   The autocorrelation function for the intensity of scattered light with a time delay τ is:

$$G(\tau) = \int_0^\infty I(t)\, I(t+\tau)\, dt \tag{1.3}$$

   The autocorrelation function for the intensity of scattered light (G) is related to the autocorrelation function for the electric field of the scattered light (g):

$$G(\tau) = 1 + \beta g^2(\tau) \tag{1.4}$$

$$g(\tau) = e^{-\Gamma t} \tag{1.5}$$

   where β is the instrumental factor and Γ is the width of the Rayleigh line.

   The mutual diffusion coefficient (D) is determined from Γ, by using the Laplace Inverse Transform. From it, the equivalent hydrodynamic radius (r) and the polydispersity can be calculated, by using the Stokes–Einstein equation:

$$\frac{kT}{6\nu\pi r} \tag{1.6}$$

k is the Boltzmann's constant ($1.038{\cdot}10^{-18}\mu$m/s$^2{\cdot}$K), T the absolute temperature (K), ν the viscosity (g/cm$\cdot$s)

Dynamic Light Scattering experiments were made with a Zetamaster Malvern. The particle size and the polydispersity of the latex particles were measured. To do it, a very diluted solution of latex is prepared. Three series of ten measurements were done for each sample.

Fraunhofer diffraction

The basic principle of the Fraunhofer diffraction is quite simple. The beam from a low power visible wavelength laser is first expanded spatially and filtered to provide a clean, parallel beam of diameter of some mm. As particles pass through the beam, they scatter or diffract the light at different angles depending upon the diameter. Large particles scatter at small angles and viceversa. Then, the scattered light is collected by lens and brought to focus on a multi-element solid state detector which

simultaneously measures the light intensity at a number of angles. The signals from the detector, usually averaged over a period of several seconds, are analyzed by the computer to give the particle size distribution. During the analysis, the sample particles move rapidly through the laser beam. As a result, they are presented randomly in all orientations giving a true average size for irregular particles. The optical system is designed such that neither the precise position nor their movement affects the disposition of the scattered light on the detector.

The experiments are made with a Mastersizer/IP from Malvern Instruments, whose laser has a wavelength of 2.40 mm. After making the background, one drop of the latex is put in the automated sample handling unit. Then the sample is automatically dispersed and diluted to the desire concentration range and the measurement is made.

Surface charge density

There are also two different ways to determine the surface charge density of the latex particles: by titration and by measuring the zeta–potential (ζ). The first one is a direct method. The charges of the latex particles are neutralized by adding ions so, at the end of the titration, the number of charges in the surface is the same as the number of added ions. The second one is an indirect method, because it needs to apply complicated equations and additional data to transform the zeta–potential values of the latex particles into their surface charge density. The accuracy of this method relies on the precision of the selected equation and the values of the required data. Moreover, this method can be applied only to diluted solutions, and its value can not be generalized to concentrated solutions, as the compact arrangements we prepared. Because of that, the first method was selected.

Titration

Three different concentration of the dialyzed latex PS were prepared. The electrolyte solution , Poly–DADMAC–Lsg solution 0.1 mM, was added. The final point of the potentiometry (streaming potential detection) is determined by a Mótek PCD 03–pH particle charge detector. This was repeated twice for each concentration. Then, a linear fit of the data was made.

The way to convert the values of volume of Poly–DADMAC into particle surface charge density is quite simple. The starting point is the usual concentration equation,

$$n = cV \tag{1.7}$$

in which c is the concentration of Poly–DADMAC solution (0.1 mmol/L), V is the volume in mL of the titration agent and n is the number (dimensionless units) of elementary charges which have been found. At the point of zero charge, this charge number must be identical to that which was at the start in the sample, on the surface of the particles. In order to express the charge in terms of coulombs, n is multiplied plus the "elementary charge constant", $1.602 \cdot 10^{-19}$ C. Finally, the charge sum must be divided by the surface of the particles in the sample. For calculating it, the solid

content weight must first divide by the particle density, in order to determine the polymer volume. This polymer volume must now be divided by the volume of a single particle, in order to determine the whole particle number, N. The surface area of the particles (A) can be calculated using

$$A = N\pi D^2 \tag{1.8}$$

where D is the particle diameter. And then, the surface charge density is calculated by dividing the charge number by the surface of the particles.

It is very important to notice that the slope of the linear fit over a latex concentration row must be used in order to get a useful value for the titration consumption, which corresponds to the point of zero charge. When this slope value is taken, it makes sense to combine this with a unreal latex concentration of 1% (w/w).

Electrophoretic mobility and zeta potential

The electrokinetic interactions between the colloidal particles determines the characteristics of the dispersion. As it was said in the introduction, the surface effects are the most important.

We are going to focus now in colloidal dispersions electrostatic stabilized, where every colloidal particle presents a charge, usually negative. When particles are highly charged, these charges produce repulsion forces between the neighbored particles. The higher the charge, the bigger the interaction. Because of that, the colloids stand on isolated and the dispersion is stable. By reducing or removing the charges, the repulsion forces are diminished and the colloidal particles agglomerate and sediment [40]. These mechanisms of aggregation are named coagulation by potential control and by electrolyte addition.

The double layer model

The colloidal particles, negatively or positively charged, are in a media which contains a lot of ions. Because of that, there are electrokinetic interactions not only between the particles but also between the particles and the ions in solution. The "double layer" model is used to explain the ionic atmosphere which evolves a charged colloidal particle. As its name says, the double layer consists of two layers of ions. The layer next to the surface is called the " Stern layer", and the other one the "diffuse layer". The ions with the same charge sign as the colloid are called "co-ions", and the ones with opposite charge are denominated "contra–ions". The Stern layer consists of a rigid layer of contra-ions, adjacent to the colloid surface. The diffuse layers is made of contra–ions, attracted by the negative colloid but repelled by the Stern layer, and also some co-ions. While the concentration of contra–ions is maxima on the colloid surface and decrease with distance, the concentration of co-ions is zero on the colloid surface and increase with it. Outside the double layer, there is an equilibrium between the cations and anions in solution. The quantity k provides the length scale for the screening, and τ=1/k, which is called the Debye length, is the thickness of the ionic atmosphere around the colloid.

Zeta potential (ζ)

The charge density is the difference of concentration between contra–ions and co–ions. It is maxima on the surface and decrease to zero in the solution. Because of that, the negative colloid and its positive charged evolvent produce an electric potential relative to the solution, which indicates the repulsive forces between colloids as a function of the distance. This potential is maxima on the colloid surface and decrease to zero outside the diffusive layer. It is not possible to determine the electric potential on the surface. However, it is defined an interesting potential in the limit between the Stern and the diffuse layer. This electric potential is denominated zeta potential (ζ). As it indicates, not only the changes in the surface potential but also the repulsive forces between colloids it is used to control and to explain the behavior of the colloidal particles.

The DLVO theory

The DLVO theory was proposed by Derjaguin, Landau (1941), Verwey and Overbeek (1943) to explain the behavior of the colloids in suspension. It is the classic approach to explain why the colloids sometimes agglomerate while other times are stable in solution. It is based on the equilibrium between the repulsive interactions (electrostatic forces) and the attractive ones (van der Waals forces).

The curve of net interaction energy is the combination of the curves of electrostatic repulsion and van der Waals attraction.(See figure 1.5). It is calculated by subtracting the curve of attraction to the curve of repulsion.

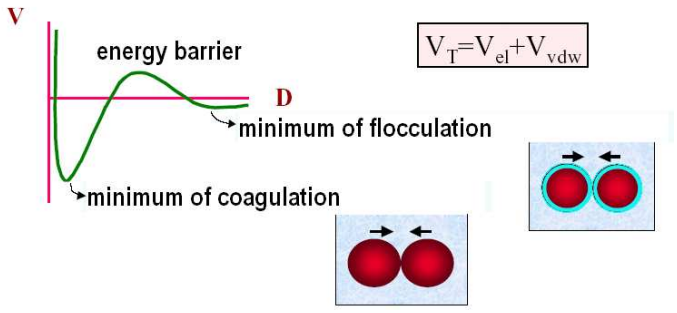

Figure 1.5: The net energy interaction curve.

The points over the abscises represent repulsive interactions and the ones below attractive. The curve changes always from attraction to repulsion and to attraction once more. The boundary, which is called energy barrier, indicates how stable is the system: when two colloids crash with enough kinetic energy to pass this barrier, their interaction become more attractive and the colloidal particles agglomerate. There are two minimum of attraction. While the relative minimum, which is called minimum of flocculation, represents a reversible agglomeration; the absolute minimum, the minimum of coagulation, is a non–reversible agglomeration.

This energy barrier can be modified by changing the ionic atmosphere, the pH

and the colloid charge among others, in order to force the agglomeration or the stabilization.

The inner region where there is no barrier is called energy trap, and represents a purely attractive interaction (systems joined by van der Waals forces).

Electrophoretic mobility

The zeta potential is usually determined by electrophoresis [41]. This electrokinetic experiment consists of applying a potential gradient to the colloidal dispersion and determining the rate of motion of the colloidal particles.

The surface charge density (σ) of a colloidal particle can be expressed as:

$$\sigma = \frac{\epsilon\zeta}{4\pi\tau} \tag{1.9}$$

The force, per square centimeter, extended to the surface is:

$$\sigma F \tag{1.10}$$

When the steady–state is reached, it is balanced by the viscous drag:

$$\frac{\eta v}{\tau} \tag{1.11}$$

where η is the viscosity of the solution and v the velocity of the particles.

$$\sigma F = \frac{\eta v}{\tau} \tag{1.12}$$

According to equation 1.12, the zeta potential of the colloidal particles can be calculated from their electrophoretic mobility:

$$v = \frac{\zeta\epsilon F}{4\pi\eta} \tag{1.13}$$

Experimental section

The experiments of electrophoresis were made in the Zetamaster Malvern. The distance between the electrodes was 8 cm and the apply potential was 150 V. The electrophoretic mobility of the colloids in this electric fields was measured in terms of V/cm.

Three different types of experiments, with several subtypes, were done:

1. Single measurements

   in water

   in NaCl 10^{-2} M

   in NaCl 10^{-3} M

2. pH measurements

   Neutral to acidic

   Neutral to basic

   Basic to acidic

3. Salted measurements

Single measurements

For experiments of single measurements, the Zetamaster MALVERN was firstly cleaned with the medium of dispersion. Then, the background intensity of scattering was checked, in order to have an optimum medium of dispersion (< 35 kCounts/ sec). After that, one drop of latex was added in 60 ml of ultra–pure water and the sample was pumped into the system . Their intensity of scattering was checked, in order to have the optimum concentration latex (< 5000 kCounts / sec). Then the mobility and the zeta–potential of the latex were measured, three times each experiment. The media used were ultra pure water, NaCl 10^{-2} M and NaCl 10^{-3} M. A glass electrode was used to control the pH.

pH measurements

For pH measurements, the Zetamaster was cleaned with the media until the starting pH presents a constant value. The air bubbles of the system were removed, one drop of latex was diluted in 60 ml of media and the sample was put into the system. The starting and final pH, and the number of measurements (12) were set. Zeta–potential and mobility were measured at several pH values.

Neutral to acidic
: The sample was diluted in ultra pure water and HCl 0.1 M was added to measure the zeta–potential and the mobility in the range of pH from 5.5 to 2.5.

Neutral to basic
: The sample was diluted in ultra pure water and NaOH 0.5 N was added to measure the zeta–potential and the mobility in the range of pH from 5.5 to 13.

Basic to acidic
: The sample was diluted in NaOH 0.5 N and HCl 0.1 M was added to measure the zeta–potential and the mobility in the range of pH from 13 to 2.

Salted measurements

For salted measurements experiments, the Zetamaster was cleaned with ultra pure water. The air bubbles of the system were removed, one drop of latex was diluted in 60 ml of media and the sample was put into the system. The number of measurements (15), the volume added (0.5 ml) and the variation factor were set. NaCl 0.5 N (pH =15) was added and zeta–potential and mobility were measured at different ion concentration depends on the variation factor, monomode (f=1) or multimode ($f > 1$, $f < 1$) experiments can be done. For the first one, the same amount of NaCl is added in each step. For the second one, their amount can be larger or smaller in every step. The multimode method is the best, when we want to focus at the beginning or at the end of the measurements.

The software used to measure and to analyze the values of zeta-potential was PCS v1.41 from Malvern Instruments.

During the coating, three different processes can take place:

1. Successful coating
   The EPMA goes to the hydrophilic surface and make a complete hydrophilic shell.

2. Partial coating
   The EPMA goes to the hydrophilic surface and make an incomplete hydrophilic shell.

3. Unsuccessful coating
   No hydrophilic shell is made, because the EPMA generates independent particles.

   The DLS and zeta–potential results allow to know how successful has been the coating. When core–shell particles diameter (BMG–24) is smaller than the hydrophobic particles (BMG–7) and their polydispersity higher, the coating has not been successful.

   In the same way, if the particles show very hydrophobic character (maximum of mobility in salted-measurements, cross–over and positive mobility in pH-measurements), the coating has failed.

1.4 Results and discussion

Figure 1.6 shows the linear fits resulted from the titration of some samples of the latex types BMG–7, BMG–60 and BMG–24 with Poly–DADMAC–Lsg(+) 0.01 mM. Three different concentrations of PS were used.

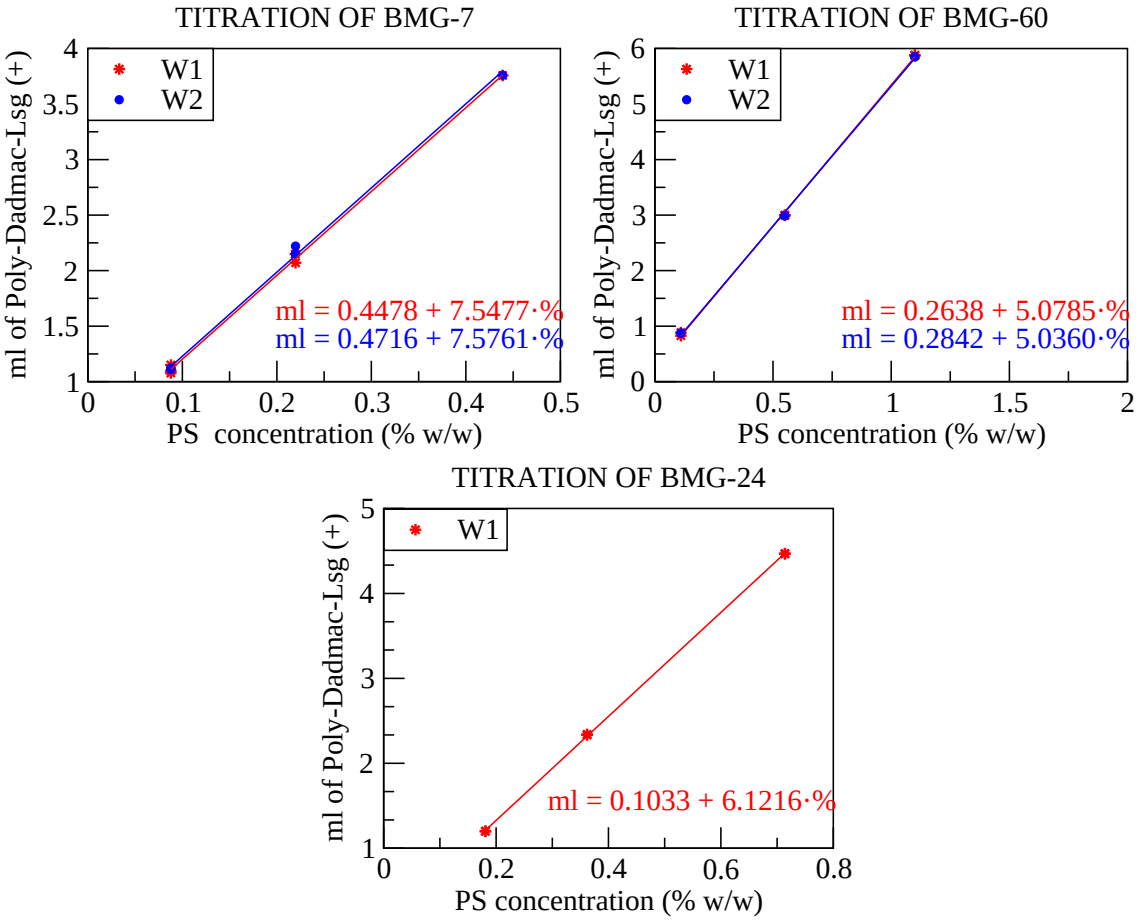

Figure 1.6: Titration of BMG–7, BMG–60 and BMG–24 with Poly–DADMAC–Lsg (+), 0.01 mM.

The surface charge density of the particles, in terms of μC/cm^2, charges(-)/particle or charges (-)/cm^2 , was calculated, with the values of the abscise in the origin and the slope of the linear fits, particle size in nm, latex density (1.054), latex concentration (0.1%), latex factor (1) and volume of the titrated sample (10 ml) (see section 1.3). These and other characteristic parameters of the synthesized latexes, before and after their purification [1], are summarized in tables 1.1, 1.2 and 1.3.

By non–aqueous dispersion polymerization (BMG–60), larger particles (about 2.5 μm) were supposed to be obtained. The reason we got in this case smaller particles could rely on Aerosol–OT (see table 1.2). The more amount of Aerosol–OT the larger size of particle. Aerosol–OT can be hydrated, so less quantity as the desire were added, so the particle size obtained was smaller.

[1] cleaned latex is the latex after applying dialysis and ultrafiltration

Table 1.1: Emulsifier–free, aqueous radical polymerization. Latex BMG–7

Sample	**[PS] (% w/w)**	**Diameter (nm)**	**Polydispersity**	**Surface charge density**
W1	4.81	1214.3	0.051	-
W1 cleaned	3.58	1180	0.047	16.62063 μC/cm^2 5366077 charges/particle $1.03749 \cdot 10^{14}$ charges/cm^2
W2	4.78	1262.4	0.054	-
W2 cleaned	4.39	1253	0.037	16.98706 μC/cm^2 5484381 charges/particle $1.06037 \cdot 10^{14}$ charges/cm^2

Table 1.2: Non-aqueous dispersion polymerization. Latex BMG–60

Sample	**[PS] (% w/w)**	**Diameter (nm)**	**Polydispersity**	**Surface charge density**
W1	9.59	1090	0.032	-
W1 cleaned	10.99	1090	0.030	9.49774 μC/cm^2 2132437 charges/particle $5.92868 \cdot 10^{13}$ charges/cm^2
W2	18.46	1070	0.048	-
W2 cleaned	19.01	1070	0.041	9.45456 μC/cm^2 2122742 charges/particle $5.90172 \cdot 10^{13}$ charges/cm^2

Table 1.3: Core shell particles. Latex BMG–24

Sample	**[PS] (% w/w)**	**Diameter (nm)**	**Polydispersity**	**Surface charge density**
W1	4.16	1293.9	0.043	-
W1 cleaned	3.62	1280.6	0.029	0.2909076 μC/cm^2 93555.74 charges/particle $1.81590 \cdot 10^{-14}$ charges/cm^2

Comparing the diameters of hydrophobic BMG–7 and core–shell BMG–24 particles and their polydispersities (see tables 1.1 and 1.3), it can be said that the coating has been successful, because the diameter increases slightly after the coating and the polydispersity decreases. That means that no new particles of EPMA were generated.

According to the literature [42], the sulfate groups of the latex surface are desionized at every pH. Moreover, only the 20% of the surface is occupied by sulfate groups, and the rest of the surface is free for ion adsorption. Because of that, the effects of the surface charge are highly smaller than the changes in the double layer of adsorbed ions, and the electrophoretic mobility of the latex depends not on the sulphates groups, but on composition of the double layer of adsorbed ions. The adsorption of ions depends on their size and polarizability. For these latex, anions are better adsorbed. So, the double layer is generally negative and the particles move to the anode (negative zeta–potential values).

As the effectiveness of the dialysis mechanism is limited, too much time is required to carry out the process completely. Because of that, particles can have slight differences in their surface charge density after synthesis and dialysis. In ultra–pure water, several parameters such as the pH or the ionic force are determined by the latex so, due to these small differences in the surface charge density of the particles, the measurements of single measurements in ultra pure water are very sensitive. In salted media, these parameters are governed by the added ions, so the mobility and the zeta-potential of the particles are more homogeneous. For this reason, measurements in ultra pure water are the best to study the chemistry of the particle surfaces, and measurements in salted media are the best ones to compare different samples.

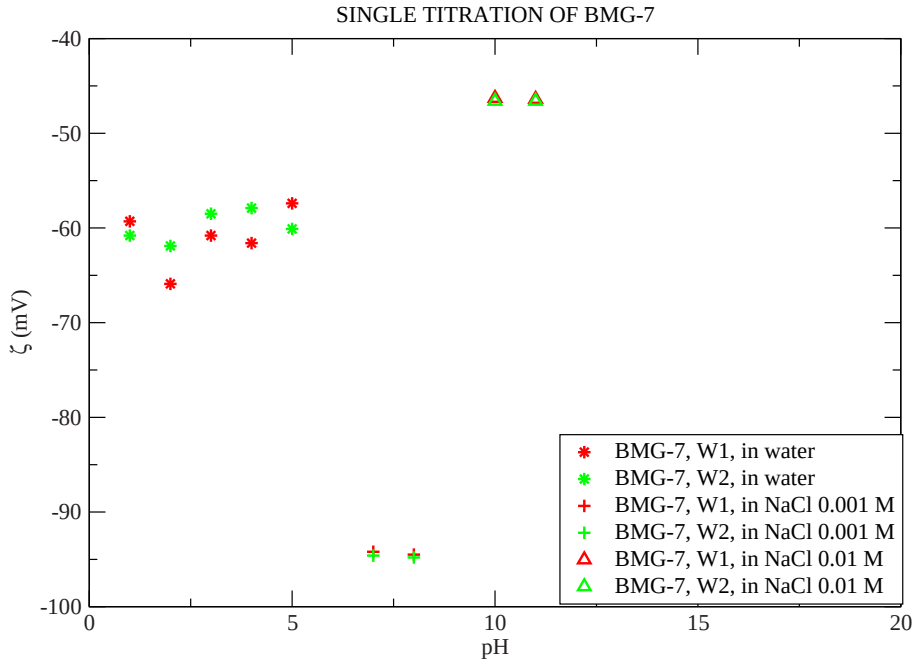

Figure 1.7: Single–measurements of BMG–7 in water, NaCl $10^{-2}M$and NaCl $10^{-3}M$.

Figure 1.7 shows the zeta–potential mobility of BMG–7 in ultra–pure water, in NaCl 0.010 M and in NaCl 0.001 M. As it is expected, the measurements in ultra–pure water, even for the same sample, present larger fluctuations than in salted media, where the reproducibility is higher. Afterwards, it can be seen that the particles present negative values of zeta–potential, which confirms the existence of a negative double layer due to the a preferential adsorption for anions.

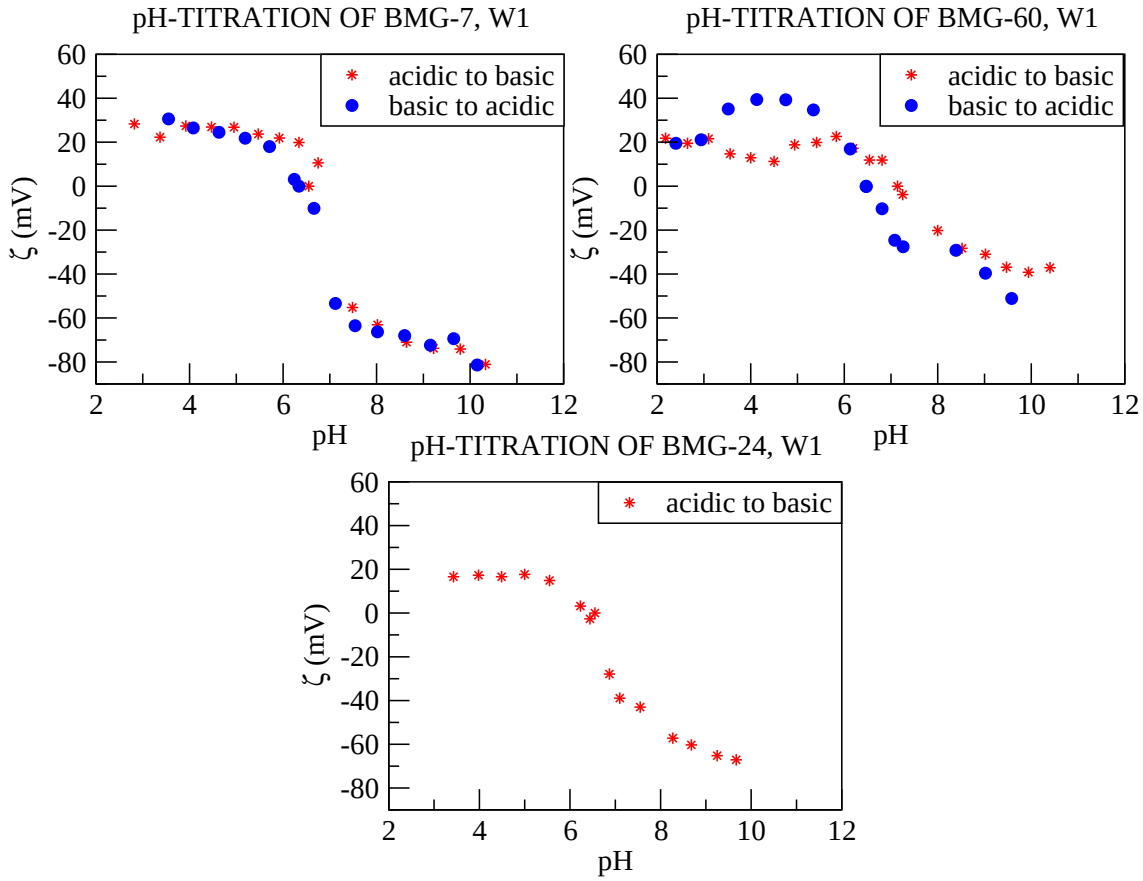

Figure 1.8: pHtitration of BMG–7, BMG–60 and BMG–24.

In figure 1.8 it is represented the electrophoretic mobility of BMG–7, BMG–60 and BMG–24 particles as a function of the pH. The concentration of anions and cations depends on the pH. The more acidic pH, the higher concentration of cations(H^+). On the contrary, the more basic pH, the higher concentration of anions (OH^-). When particles present free surface to adsorb ions from the media, their double layer changes due to this adsorption, and a typical sigmoidal curve is observed when plotting electrophoretic mobility versus pH. This behavior is observed for BMG–7 and BMG–24, because these particles are smooth, and can be explained as following: in basic conditions (pH>7), particles show big and negative zeta–potential values due to the adsorption of OH^- anions. The more anion adsorption, the higher mobility. As the hydrophilic shell of BMG–24 particles reduces ion adsorption, it is expected that BMG–7, which is hydrophobic, presents higher mobility than BMG–24 (more negative values of electrophoretic potential). This is confirmed by comparing

the first and the third graphics of figure 1.8.

By decreasing the pH, the number of anions decreases as the same time as the number of cations increases. The composition of the double layer changes, due to ion exchange, and the mobility of the particles decreases. When there are more cations adsorbed than anions, the double layer becomes positive and particles move to the cathode, with positive zeta–potential values. This positive mobility increases at acidic pH (pH<7), because the number of cations increases. The point of zero mobility is called cross–over. The more sulphate groups on the particle surface, the more acidic pH. In this way, this is a good method to determine the percentage of occupation of sulphate groups.

On the other hand, only hydrophobic smooth particles, which present a huge free surface for adsorption, are able to adsorb positive ions since particle roughness or hydrophilic shell avoid cation adsorption. Because of that, BMG–60 and BMG–24 should not present neither cross–over nor positive mobility and, at acidic pH, their electrophoretic mobility should stand at zero instead. However, the second and the third graphic of figure 1.8 show that BMG–60 and BMG–24 present positive mobility, which means that the ion adsorption in these latexes is higher than the theoretically expected. In the case of BMG–24, this fact reveals that the coating with EPMA was not completely successful and BMG–24 particles present an incomplete hydrophilic shell, which allows to adsorb more ions.

In principle, the same curve should be obtained when the measurements are made from acidic to basic pH and from basic to acidic pH. However, comparing both curves, small fluctuations in the zeta–potential values can be detected at acidic pH. This effect is observed because the adsorption of cations in acidic pH can be slower as the ion exchange. To avoid this, is better to do the measurements from basic to acidic pH to let the cations have more time to be adsorbed.

Due to the roughness of BMG–60 particles, ion adsorption is strongly reduced and their electrophoretic mobility should stand at zero at any pH. However, the second graphic of figure 1.8 shows both negative and positive values of it. This deviation from theory is caused by the PKV and Aerosol–OT chains, negatively charged, which can be extended in the media in different configurations. The negative mobility of the particles at very basic pH is extremely high. This is not caused by ion adsorption (this rough latex can not adsorb so many anions), but by the negatives charges of PKV and Aerosol–OT chains, which are extended in the media. The hysteresis observed in these two curves is too high and is caused by the different configurations that the lateral chains can adopt. The cross-over, the positive mobility at acidic pH and its fluctuations are also caused by the chain charge.

Figure 1.9 shows the zeta-potential values of the synthesized latexes obtained by salted measurements. The negative mobility of the particles confirms the existence of a negative double layer, due to the adsorption of anions. The more anion adsorption, the higher mobility. Firstly, the zeta–potential of BMG–7 and BMG–24 particles increases with the salt volume until a maximum of mobility, after which it decreases. This behavior is caused by changes in their double layer. At the beginning, all the ions added are adsorbed by the latex, since there is free surface for the adsorption. Due to this ion adsorption, the double layer is expanded and

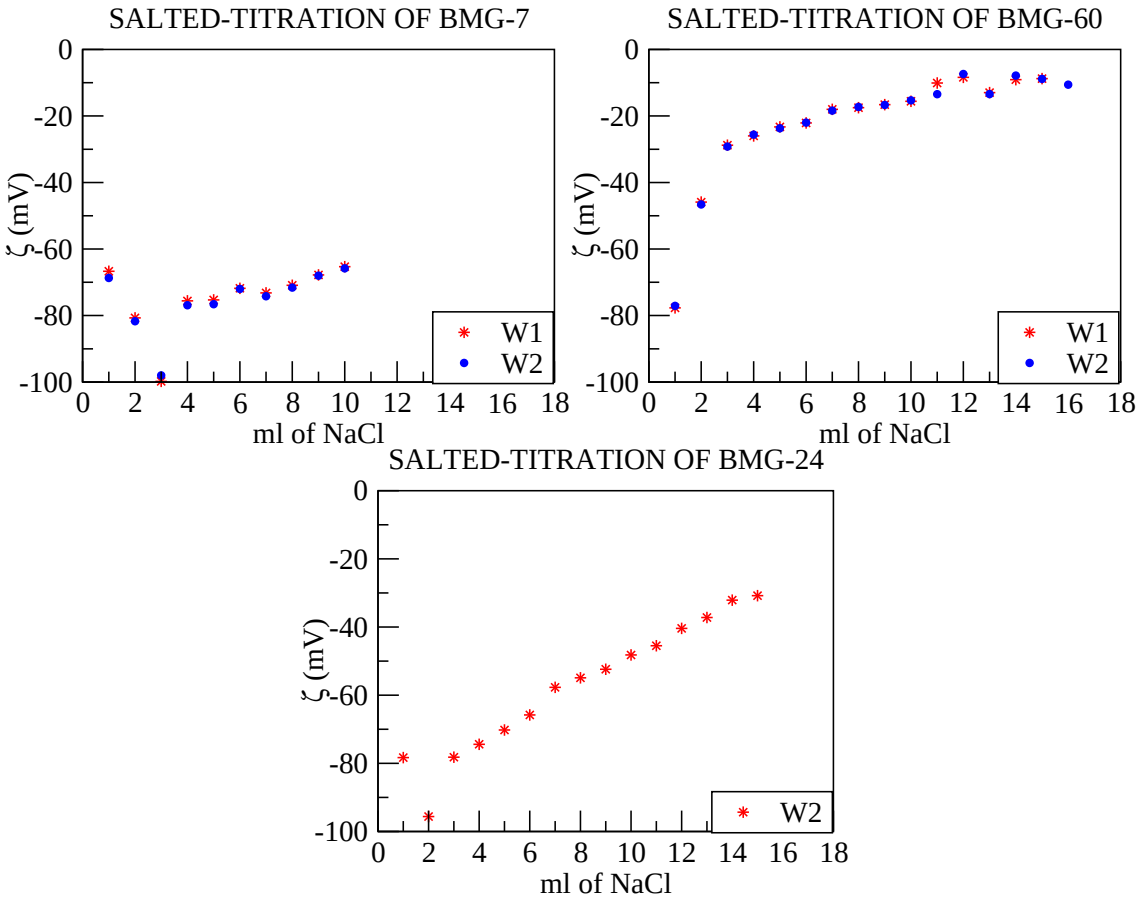

Figure 1.9: Salted–titration of BMG–7, BMG–60 and BMG–24.

the mobility of the particles increases. When the number of added ions is large enough, not all of them can be adsorbed and those which can not, remain between the particles and the electrodes. This screening effect compress the double layer, and the mobility of the particles decreases. This maximum of mobility is one of the best parameters to recognize hydrophobic or smooth particles, which have free surface for ion adsorption. As the hydrophilic shell of BMG–24 particles reduces the possibility of ion adsorption, the mobility of BMG–7 particles reaches higher values than the BMG–24, as well as their maximum of mobility.

When there is no free surface for ion adsorption, the added ions compress the double layer from the beginning and a monotonous decrease of the zeta–potential is observed. This behavior takes place for hydrophobic rough particles, such as BMG–60, and also for too–charged particles (occupation > 50 %). As it has been yet mentioned, these measurements are very useful not only to determine the hydrophobic character of the particles or their roughness, but also the percentage of occupation of sulphate groups. BMG–60 particles show no maximum of adsorption. The surface of these particles contains chains of PKV and Aerosol–OT, which make them be hydrophilic and rough and also are responsible for several anomalies in the results. The starting mobility, which is high for hydrophilic particles, is caused not

because of the ion adsorption, but for the negatives charges of the Aerosol–OT and the PKV, which extend their chains in the media. When we add ions to the media, they first neutralize the charges of the Aerosol–OT and the PKV, and once these charges have been neutralized, the mobility decreases appreciably.

According to the literature [22; 44; 45], the PS particles used in self-assembly are the hydrophobic, smooth and charged ones, stabilized by electrostatic repulsion, and prepared by classical emulsion polymerization techniques. Because of that, BMG–7 was the first type of latex that we have prepared. In this particular case of large particles, the particle surface charge density required to stabilize them was very high. Because of that, we sometimes observed cases of plastification and coalescence (film formation) during the first stages of the vertical deposition. In order to avoid these problems, we decided to reduce the surface charge density of the particles. This fact made us think of stabilizing the latex by another type of method different from electrostatic repulsion, and finally we decided to prepare a latex sterically stabilized.

From this point of view, we made a second attempt with the latex BMG–60, which consist of hydrophobic, rough and uncharged particles, sterically stabilized. The problem of plastification was solved, but the behavior in solution of these particles depended more of the Aerosol–OT and PKV chains than of the double layer of ions. Because of that, it was not easy to control and then we decided to prepare another type of particles, which joined the best characteristics of BMG–7 and of BMG–60.

In this way, were synthesized the BMG–24. This latex consists of hydrophilic, smooth and charged particles, both electrostatically and sterically stabilized. The electrophoretic mobility of this latex is similar to the ordinary hydrophobic and smooth latexes (BMG–7), but the plastification is avoided by sterical effects and by its hydrophilic character.

After developing this systematical study of the electrokinetic properties of these three different types of latex, we can say that for large particles, it is necessary to stabilize the dispersion not only by electrostatic repulsion but also by sterical effects. It is also important to notice that the stabilization with hydrophilic polymer chains (tentacles) improves the self–assembly of large particles.

Chapter 2

Colloidal crystallization

2.1 Vertical deposition

The mechanism of the vertical deposition technique (*the Dimitri–Colvin method* [43; 44]), relies on the balance between solvent evaporation rate and particle sedimentation. Consequently, for a certain particle size the sedimentation is faster than solvent evaporation and in this case the self–organization of the particles does not take place. That means that self–assembly is only possible for a proper balance between both effects above mentioned. For particles smaller than 400 nm, successful conditions are relatively easy to achieve [44], but larger particles sedimented too quickly and successful conditions exist only in narrow ranges of the parameters of control. The rate of evaporation can be controlled by type of solvent and temperature [45] and the rate of sedimentation, by solvent and material density and by convective flows [46].

Under the optimal conditions, evaporation of the solvent leads to the deposition of an ordered three dimensional packing of more or less uniform thickness on the substrate, starting from a position below the initial level of the contact line at the top of the meniscus. After the opal is dried, the polymeric spheres adhered well enough to each other and to the substrate, so the film can be easily handled or even re–immersed in solvent without detaching or destroying.

2.1.1 Experimental section

Substrates and material

Hydrophobic PS latex particles with a narrow size distribution and a diameter of 1 μm (BMG-24) and 1.4 μm (PS34) were prepared by an emulsifier–free, aqueous radical polymerization [34; 35]. These colloids were coated with a hydrophilic shell by a procedure described in [36] to increase their stability. Large, uncharged PS sterically stabilized tentacle particles with a diameter of 2.8 μm (BMG–60) were prepared by non–aqueous dispersion polymerization [47]. The refractive index of the particles is 1.59.

Aqueous ammonium hydroxide (25% V/V) was provided by PANREAC and

hydrogen peroxyde (30% V/V) by Merk.

Pure (>99%) glycerol, ethylenglycol–monobutylether, N–methyl–2–pyrrolidon, dipropylenglycol–dimethylether and dipropylenglycolmethylether–acetat were provided by Aldrich. Pure diethylenglycol–dimethylether by ACROS.

Ultra pure water, 1 μS/cm conductivity, was used from a Mili–Q water system, and also ultra pure heavy water, D_2O.

Commercial ultra sounds cleaner for optic material, OPTIC II SUPER, is provided by Technological.

10x26 mm glass slides provided by Roth Karlsruhe were used as substrates, and also silicon slides of 10x26 mm.

Method

All dispersions were diluted with ultra pure water to concentrations between 0.1 and 1%(w/V) and mixed by applying ultra sounds 10 minutes at half power and room temperature, before use. When the latex was not recently synthesized, it was previously filtered using a 8 μm filter.

Glass slides and silicon slides (12 mm x 25 mm, thickness 1mm) were used as substrates. They were perfectly cleaned and the method used depends on the type of material. Glass substrates are cleaned in three steps. First, by putting them 10 minutes at room temperature in an ultrasound bath SONOREX SUPER DIGITAL 10P (BANDELIN). After that by hydrophilization, introducing them in a glass with a 1:1:5 mixture of ammonium hydroxide, hydrogen peroxide and water for 30 min at 67°C. The heat is applied by a RCT basic and temperature controlled by a IKATRON ETS 03, both of them from IKA LABORTECHNIK. And finally, intensive rinsed with ultra pure water. Silicon substrates were cleaned by two different methods. The first one consists on applying pressure air and the second one on applying pressure air, hydrophilization and rinsing with ultra pure water.

In a representative procedure, the substrate was placed approximately vertical in a cylindric plastic vial (inner diameter, ca. 13 mm; volume, 2.5 mL). Then the vial was filled with approximately 1.5 mL of particle suspension and taken in a thermobank COESFELD Thermostair, which controlled the temperature. Normally, as the slide was slightly declined deposition of the particle array occurred mostly on the one side of the glass. (Figure 2.1)

Parameters of control

There are some parameters which allow to control the solvent evaporation rate.

1. Type of solvent
   Ultra pure water, water/ethanol mixtures, water/heavy water mixtures or water with co–solvents as glycerol, ethylenglycol–monobutylether (butylglycol, BG), N–methyl–2–pyrrolidon (NMP), dipropylenglycol–dimethylether (DPGDME), diethylenglycol–dimethylether (2–methoxyethyl ether, DEGDME) and dipropylenglycolmethylether acetat (DPGMEA) were studied as mediums of deposition.

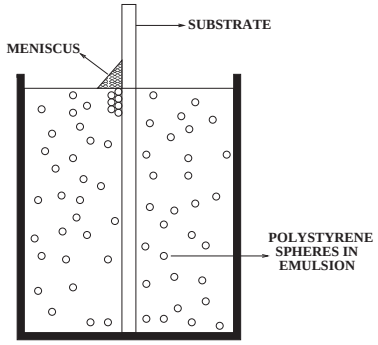

Figure 2.1: Scheme of the vertical deposition method

2. Temperature
   The temperature has been ranged from 40° to 80°

Another parameters allow to regulate the sedimentation of particles.

1. Particle size
   Particles of 1.4 and 2.8 μm diameter size were studied

2. PS concentration
   It has been studied in the range from 0.1 to 1 %(w/V)

3. Substrate
   Not only the kind of substrate but also the method to clean it before the deposition are critical in the vertical deposition. Glass and silicon are used as substrates, and hydrophilization and commercial ultra sounds cleaner as ways of cleaning.

Experiments done

The nomenclature used consists on numbers and letters, which are used only with the parameters of control. The numbers before the point refers to the set, the second pair of numbers to the concentration and the third pair to the temperature. When the medium or the solvent were parameters of control, its first letter is used to specify it.

In table 2.1 are summarized all the samples prepared by vertical deposition, with their corresponding conditions of deposition.

Table 2.1: Samples prepared by vertical deposition.

Set	Substrate	Particle size (μm)	[PS] (%w/V)	Temperature (°C)	Solvent	Sample
1	hydrophilized glass	1.4	0.1–1	40–70	water	1.0140–1.0170 1.0240–1.0270 1.0540–1.0570 1.140–1.170
2	hydrophilized silicon[1] non–hydrophilized silicon	1.4	0.1	60–75	water	2.A60–2.A75 2.H60–2.H75
3	hydrophilized glass	1.4	0.1	70	water/ ethanol[2] (0–100%)	3.A–3.G
7	hydrophilized glass	1.4	1	70	water/ co–solvents[3] (1%)	7.W 7.G 7.NMP 7.DPGDME 7.DEGDME 7.DPGMEA
8	hydrophilized glass non–hydrophilized glass[4]	2.8	1	65–80	water	8.H65–8.H80 8.U65–8.U80
9	hydrophilized glass	1.4	1	70	water/ co–solvents (0.25–2%)	9.G025–9.G2 9D025–9.D2
10	hydrophilized glass	2.8	0.1–1	40–55	water/ heavy water (1:1)	10.0140–10.0155 10.02540–10.0255 10.0540–10.0555 10.140–10.155
11	hydrophilized glass	1	0.1–1	60–70	water	11.0160–11.0170 11.0260–11.0275 11.0560–11.0575 11.160–11.175

2.1.2 Characterization

Colloidal crystals with large particles (diameter>0.7 μm) show their stop–band into the NIR and IR region. In this way, optical properties of the polystyrene colloidal single–crystal films were evaluated by measuring their transmission spectra at normal incidence and reflection spectra at different angles of incidence, using a Research Series FTIR UNICAM spectrometer from Thermo–Nicolet.

The basic features of the normal incidence optical spectrum of these colloidal crystal multilayers can be predicted by a simple diffraction theory. When the wavelength of incident light satisfies the Bragg condition, it is diffracted away from the propagation axis, leading to a decrease in the transmission and thus a peak in the absorption spectrum. The position of this peak can be related to the particle diameter and the refractive index of the medium using:

$$\lambda_{max} = 2n_{eff}d_{111} \tag{2.1}$$

[1]H indicates hydrophilized silicon slides and A the ones cleaned by pressure air.

[2]A was used for the sample made in ultra–pure water and G for the one fabricate in ethanol. B, C, D, E and F were used to denominate the samples prepared in medium with increasing rates of ethanol/water (1/6 to 5/6, respectively).

[3]W indicates water and G glycerol

[4]H indicates hydrophilized and U non–hydrophilized glass slides.

where n_{eff} is the refractive index of the medium, which is given by a volume–weighted average:

$$n_{eff} = \sqrt{\Psi n_{PS}^2 + (1 - \Psi) n_{air}^2} \tag{2.2}$$

with

$$n_{PS} = 1.5683 + \frac{10087}{\lambda^2} \tag{2.3}$$

and Ψ is the volume fraction occupied by the polystyrene spheres, which is approximately 0.74 for close–packed spheres. d_{111} is the interlayer spacing for (1 1 1) planes, which is related to the sphere diameter (D). For close–packed spheres:

$$d_{111} = \left(\frac{2}{3}\right)^{\frac{1}{2}} D \tag{2.4}$$

While this simple diffraction theory can predict the peak positions, it is unable to provide a quantitative explanation for any of the other features in the spectra, like their amplitude. In the 90's, several groups attempted to adapt the dynamical theory of X–Ray diffraction to this purpose ([48; 49; 50; 51; 52; 53]).

However, this dynamical theory is based on the approximation that the refractive index contrast between the scattering centers and the intersticial medium is quite small, of order of 10^{-4}, an approximation not valid for these polystyrene–air crystals. For this reason, a detailed analysis of the shapes and intensities of the optical transmission functions require more complete treatments of scattering from periodic dielectrics. Theories of the optical properties of photonic band gap materials provide an avenue for this understanding [54].

An important feature of these spectra is the rising background that grows at shorter wavelengths; this causes the samples to look slightly hazy and could place limits on their use in many optical applications. This background has been observed but rarely discussed. While it does not clearly fit the λ^{-4} dependence expected for Rayleigh scattering, defects or sphere roughness could give rise to this phenomenon. Alternatively, it may represent the collective effect of the diffraction of all the lattice planes other than (1 1 1) planes [55]. If so, it is an intrinsic property of any periodic arrays of spheres, not merely of self–assembly colloidal crystals.

An interesting feature of the optical spectra is the increase in peak width as sample thickness is decreased. This effect is similar to the Debye–Scherrer broadening of X–Ray diffraction peaks in small crystallites [56].

Multilayer thickness is an important parameter for quantitative assessment of sample optical properties. Although scanning electron microscopy (S.E.M.) provides a measure of this parameter, it is a destructive method, since it requires the deposition of a gold coating on the sample to obtain high quality images. For large particles (>1 μm) the number of layers can also be determined by optical microscopy, by focusing carefully the different layers. A less time–consuming and nondestructive method is an optical technique which uses the Fabry–Perot (FP) fringe ([57; 44]) positions to analyze the film thickness. These fringes result from interference between reflections from the top and the bottom surfaces of the sample. An analysis,

using Bragg law's, of the spectral positions of theses local maxima allows an accurate determination of the sample thickness.

At normal incidence, one particular FP maximum occurs at a wavelength, λ_l given by:

$$p_l \lambda_l = 2 n_{eff} T \tag{2.5}$$

Here, p_l is an integer and T is the film thickness.

Subsequent maxima appear at shorter wavelengths:

$$(p + p_l)\lambda_p = 2 n_{eff} T \tag{2.6}$$

where p is a positive integer numbering consecutive maxima from the long–wavelength fringe, p_l. Rearranging the equations gives the film thickness, T:

$$T = \frac{p \lambda_p \lambda_l}{2 n_{eff} (\lambda_l - \lambda p)} \tag{2.7}$$

Thus, a plot of p with

$$\frac{2 n_{eff} (\lambda_l - \lambda p)}{\lambda_p \lambda_l} \tag{2.8}$$

gives a straight line with a slope of T.

This technique can not measure film thickness greater than 8 μm when using visible light. As it was previously commented, the width of the Fabry–Perot fringes decreases with increasing film thickness, eventually becoming too small to be measured.

According to Colvin et al. [58], the intensity of the peak is related with the number of layers, the more number of layers, the higher intensity. This increase is smooth and monotonic, and contains no evidence of a threshold thickness for the formation of a stop band.

In contrast, the width of the stop band presents a more dramatic dependence on film thickness. The observed narrowing of the stop band with increasing film thickness is similar to the Debye–Scherrer effect in X-ray diffraction. Here, the angular width of a diffraction line is limited by the highest spatial frequency accessible to the reciprocal lattice. Because of that, the width is inversely proportional to the number of lattice planes, and narrower lines are obtained by increasing the crystal thickness. In the practice, the narrowing of the stop bands saturates above a certain value of thickness.

This understanding of the nature of the stop bands offers an idea to prepare materials with narrower bandwidths, useful for engineered photonic systems. As the bandwidth is sensitive function of the dielectric constant (see equation 2.7), these materials can be synthesized by filling the intersticial pores of the colloidal crystals with other materials.

Also, these colloidal crystals are expected to diffract light at a wavelength given by Bragg's law, modified to account to refraction

$$\lambda = 2 d_{hkl} \cdot \sqrt{n_{eff}^2 - sin^2(\alpha - \theta)} \tag{2.9}$$

where d_{hkl} is the distance between two crystallographic planes parallel to the surface; n_{eff} is the effective (average) index of refraction, α is the angle between $(h_1k_1l_1)$ and $(h_2k_2l_2)$ planes and θ is the angle of incidence.

$$d_{hkl}^2 = \frac{a^2}{(h_2k_2l_2)} \tag{2.10}$$

where a is the lattice parameter,

$$a = D\sqrt{2} \tag{2.11}$$

$$\alpha = arcos\left(\frac{h_1h_2 + k_1k_2 + l_1l_2}{\sqrt{(h_1^2 + k_1^2 + l_1^2)(h_1^2 + k_1^2 + l_1^2)}}\right) \tag{2.12}$$

In reflection spectroscopy, the dependence of the peak wavelength (λ) on the incidence angle (θ) can be fitted to this equation, to determine the effective refractive index of the sample and the size of the particles.

Using large particles (diameter>0.7 μm) have also the advantage to be easily visualized by optical microscopy. Because of that, optical orthoscopic and conoscopic (with Bertrand lens) micrographs were performed with an OLYMPUS BX60, equipped with a CCD–device (SONY camera adaptor CMA–D2). (See figure 2.2).

The application of a Bertrand lens allows the direct visualization of Fraunhofer diffraction patterns and was first introduced for the investigation of particle monolayers by Pinnow [59] and also recently used ([60; 61]). In this optical arrangement diffraction phenomena appearing in the focal plane of the microscope objective are directly viewed by the so–called Bertrand–Amici lens through a CCD color camera [62]. The resulting pictures show the effects of diffraction of light at the individual lattice planes of the crystalline particle array and, if white light is used, of light dispersion (due to diffraction) into the colors of the optical spectrum. Therefore, this diffraction technique is a useful tool for the study of the optical properties of ordered particle arrays.

Nowadays, only the diffraction patterns produced by a single monolayer can be successfully explained by the theory. Several directions of diffraction are expected such as the (1 0)–, (1 1)–, (2 1)–directions (see figure 2.3).

Optical microscopy was used to determine the size of domain and the number of layers. The first one was made by image processing of the micrographies, using the commercial software ANALYsis 3.0, and the microscopic diffraction technique (single domain diffraction of white light) to make a systematical study of the diffraction patterns of different crystalline geometries and packing.

RGB–Intensity profiles were made by representing the distribution of light intensity (for the red, green and blue colors) in a specified direction of the diffraction pattern. The intensity profiles of diffraction in the (1 0)–direction were mainly studied.

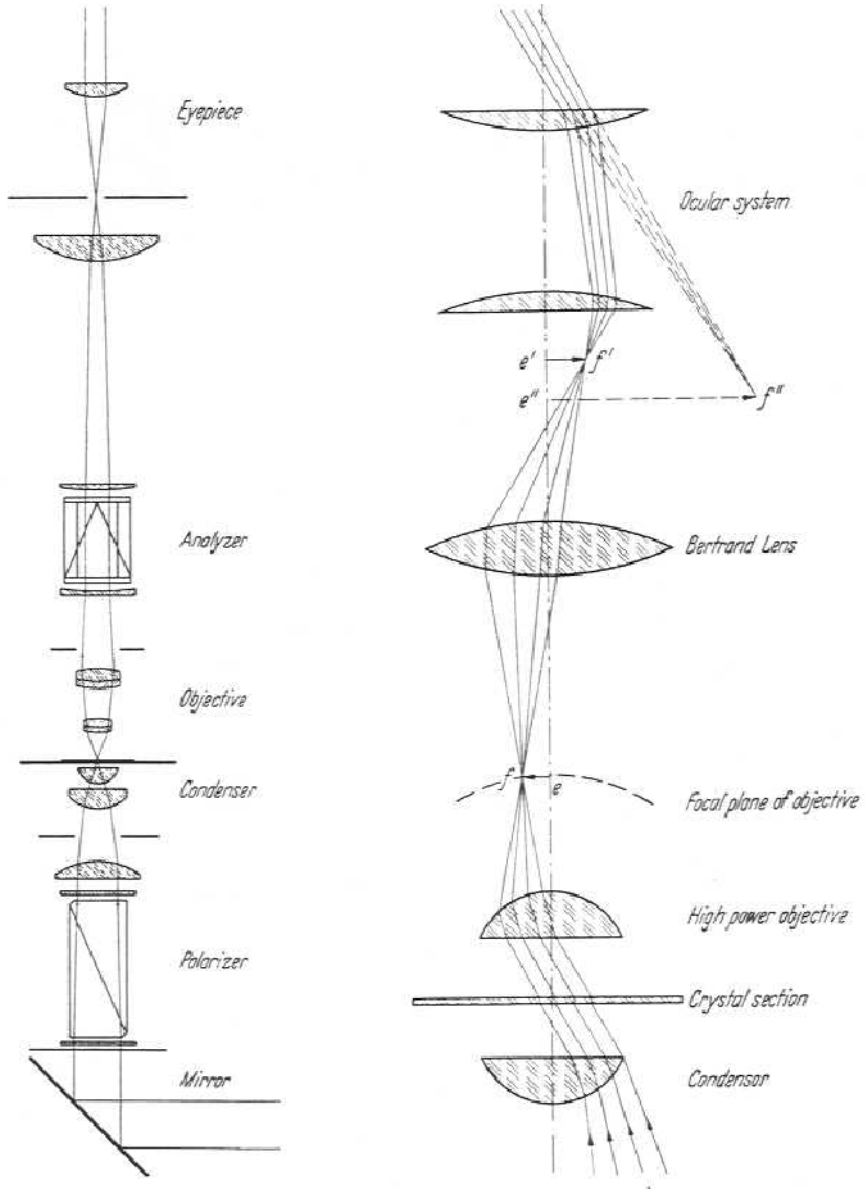

Figure 2.2: The polarizing microscope. Left: Light rays for orthoscopic (normal) arrangement. Right: Light rays for conoscopic arrangement, using Bertrand lens.

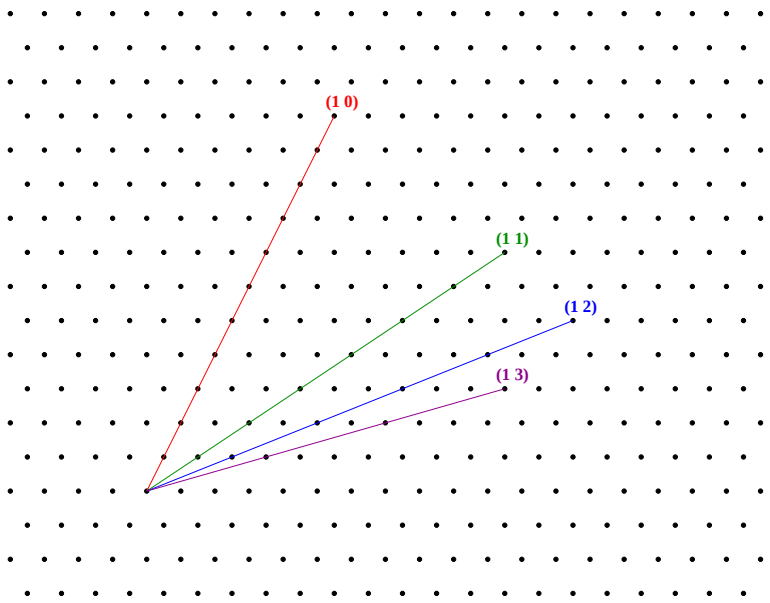

Figure 2.3: Diffraction directions from a monolayered arrays.

Calibration of the microscope and CCD–device

In order to make quantitative measurements, calibration is needed. Figure 2.4 shows the scheme used to make the calibration, which was made in seven steps:

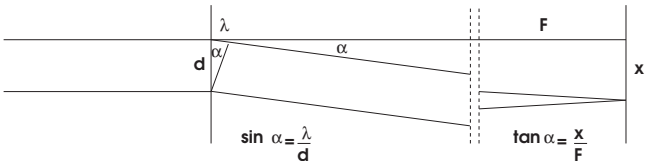

Figure 2.4: Calibration of the microscope/CCD–device.

1. Calibration of distance measurement in x and y directions by means of the etalon, for 10, 20, 40, 100 and 250 magnification.

2. Determination of the grating constant (d) of the line grating.

3. Determination of the virtual image distance (F) for each objective by means of the line grating and an interference filter of given wavelength λ

$$F = \frac{x}{tan\left(arcsin\left(\frac{\lambda}{d}\right)\right)} \tag{2.13}$$

4. Find a general relation between F and the magnification of the objectives.

$$F = A + B \cdot \frac{1}{mag^2} \tag{2.14}$$

In our experimental setup, A = 3.1124 and B = 14179.

5. Do the white balance of the CCD–camera for standard illumination.

6. Determination of the wavelength λ_R, λ_G, λ_B for the RGB–extractions of the CCD–camera.
$$\lambda_{R,G,B} = d \cdot sin\left(arctan\left(\frac{x_{R,G,B}}{F}\right)\right) \tag{2.15}$$
In our optical device, R =595 nm, G = 532 nm and B = 463 nm.

7. Determination of the image deviation function for high diffraction angles α.

2.1.3 Results

Influence of the temperature and the PS concentration

Macroscopically, the samples prepared are not uniform but showed the characteristic appearance in stripes, typical from the vertical deposition. This is caused because the number of deposited layers is different along the substrate. As the temperature is constant, both the solvent evaporates and the meniscus goes down at a constant velocity. Because of that, the thickness of the sample was expected to be either constant or to present a monotonous change. The reason for this unexpected fact could be that they are changes in the concentration of particles at the meniscus due to gradients of concentration or due to convective cycles caused by gradients of temperature.

The systematic change in color seen in transmission and reflection of uniform films of different particle sizes is due to Bragg diffraction. Optical images of the top view of these samples show that the colloids are arranged in a close–packed arrangement, where each sphere touches six others in one layer. This close packing arrangement is well–known in colloidal crystals, such as these polystyrene spheres, whose ionic interactions are minimal. These images illustrate that the samples are oriented with their (1 1 1) plane parallel to the substrate (see figure 2.5).

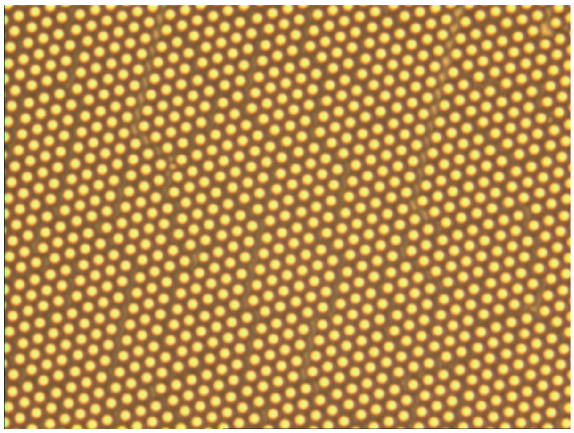

Figure 2.5: Optical micrography of sample 1.170 made with 2500 increases.

In this close–packed geometry, whether the structure can be face–centered cubic (ABCABC ...), hexagonal close–packed (ABABAB ...) or randomly stacked (ABABCA ...), the first one was found in the most of the cases (see figure 2.6).

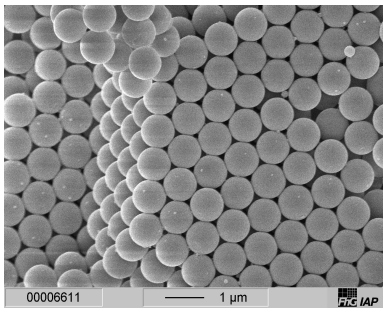

Figure 2.6: S.E.M. micrography of sample 11.170 made with 10000 increases.

The arrays are hexagonal, except from the transition areas from one to two layers (or from two to three), where cubic arrays are observed. In the transition areas, the number of layers is fractional (1.5, 2.5, ...). While the hexagonal arrangement is the most stable for a packing of spheres in "complete layers", cubical arrays seem to be the most stable for "fractional layers". According to Lazarov et al. [63], cubic arrays take place when particle array go from one to two layers. Sometimes, mixed arrays are also observed (figure 2.7).

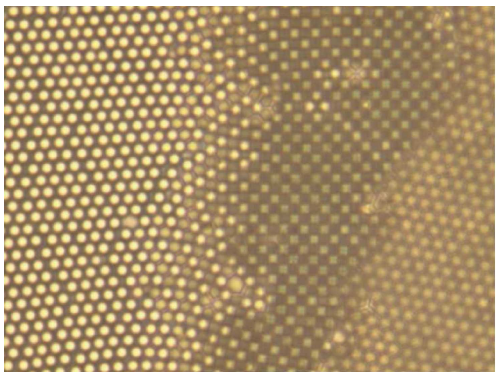

Figure 2.7: Cubic transition from a monolayer to a bi layer, found in sample 1.0570.

By optical microscopy the domain size and the number of layers of the samples were determined. The micrographs showed that neither temperatures lower than 70°C nor PS concentrations smaller than 0.5% (w/V) are proper to make vertical deposition. For temperatures lower than 60°C, particle sedimentation is faster than solvent evaporation and in this case the self–organization of the particles does not take place, at least for the large particles investigated. Because of that, small domains are observed by optical microscopy in these samples.

Only a few layers were deposited in all the cases. The higher PS concentration, the more layers deposited and the bigger domain size. It was also observed that, for the same PS concentration, the higher temperature, the bigger domain size (figure 2.8). In this way, to obtain good monolayers low concentrations and high temperatures were needed.

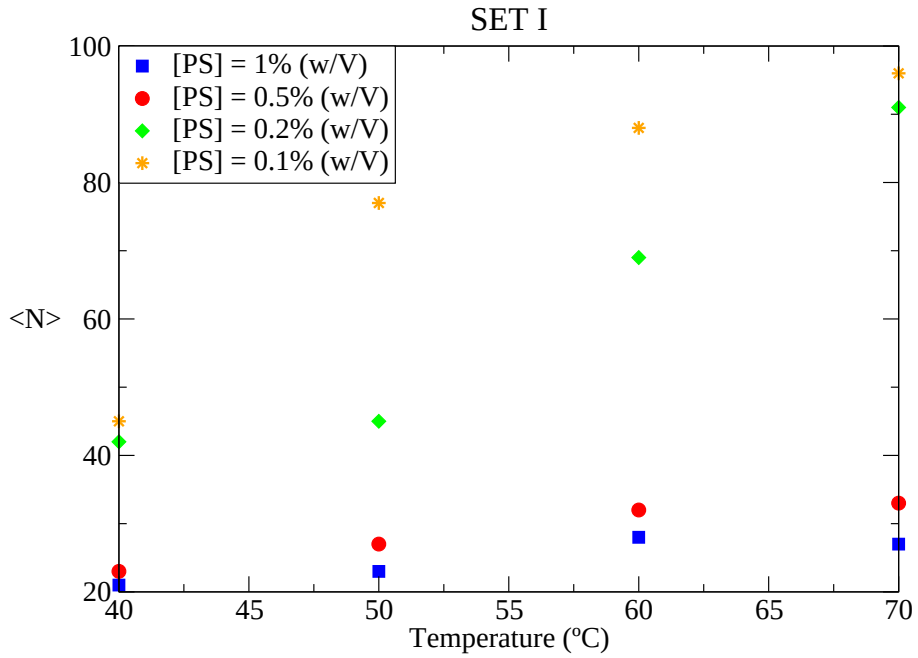

Figure 2.8: Average size of domain $< N >$ of the top layer vs. temperature, for different concentrations of PS. Set 1: samples 1.0140 to 1.170

The results confirm that using low latex concentration is the way to obtain optimal monolayers, and that applying high temperatures is needed to prepare colloidal crystals with large domains.

Substrate

Optical micrographs of the samples were taken and the results are shown in figure 2.9. It can be seen that better samples were obtained on hydrophilic substrates. Because of that, the self–assembly of PS colloidal particles seems to be improved by first hydrophilizating the substrates.

The degree of hydrophilization was checked by putting a drop of water on the substrate. The more hydrophilic substrate, the more water stands on it.

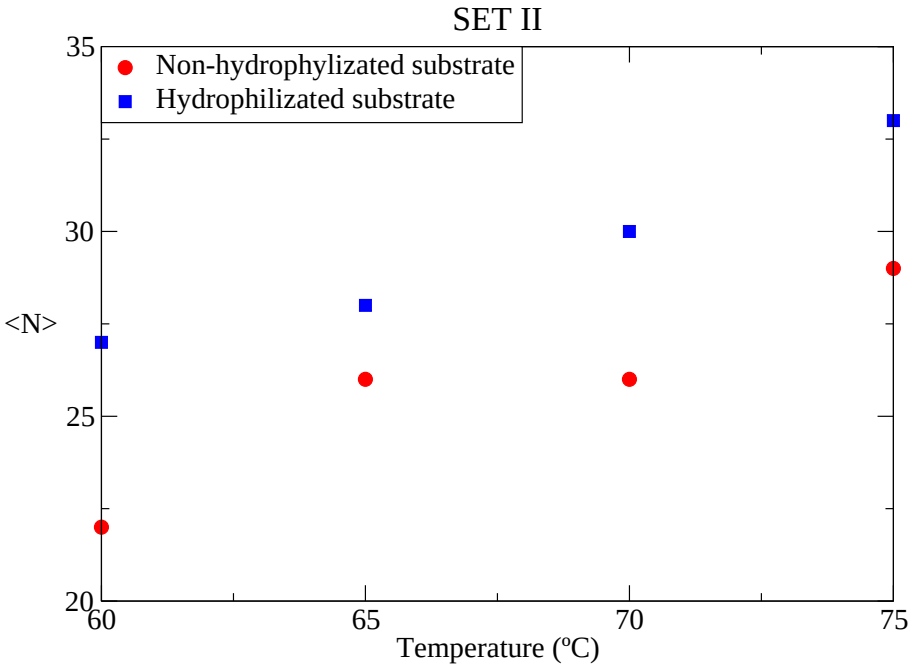

Figure 2.9: Average size of domain of the top layer ($< N >$) vs. temperature, for different methods of preparation of the substrates. Set 2: samples 2.A60 to 2.H75

Solvent

The results of set 3 show that the higher percentage of ethanol, the bigger size of domain, until 50% from which the solvent evaporation is too fast and sedimentation of the particles is done without self–organization. This can be seen in 2.10.

One of the biggest problems of colloidal crystallization is the formation of cracks (see figure 2.11).

In order to reduce the number of cracks, the crystallization was made in different media such as water, ethanol, water–ethanol mixtures and water with different co–solvents. Besides it was studied the influence of the medium in the crack formation. The results of set 8 show that glycerol and DPGDME are the best co–solvents, as they reduce appreciably the number of cracks formed during the drying stage (figure 2.12). As the co–solvents are not volatile at room temperature, they remain between the ordered particles in the colloidal crystal, avoiding the drying stage. As there is no drying stage, no cracks are formed. By these way, we do not prepare dry colloidal crystals, we make wet colloidal crystals instead. It is important to notice that few co–solvent is used, in order to prepare structures where the attractive forces between particles (the ones which make the structure stable) are strong enough.

The particle swelling in the other co–solvents is stronger. Because of that, the glass transition temperature (T_g) of the PS decrease (plastification) and coalescence (film formation) takes place during the deposition. So, the other co–solvents not only not reduce the number of cracks, but also form a thin film over the surface, which makes the characterization much harder (see figure 2.13).

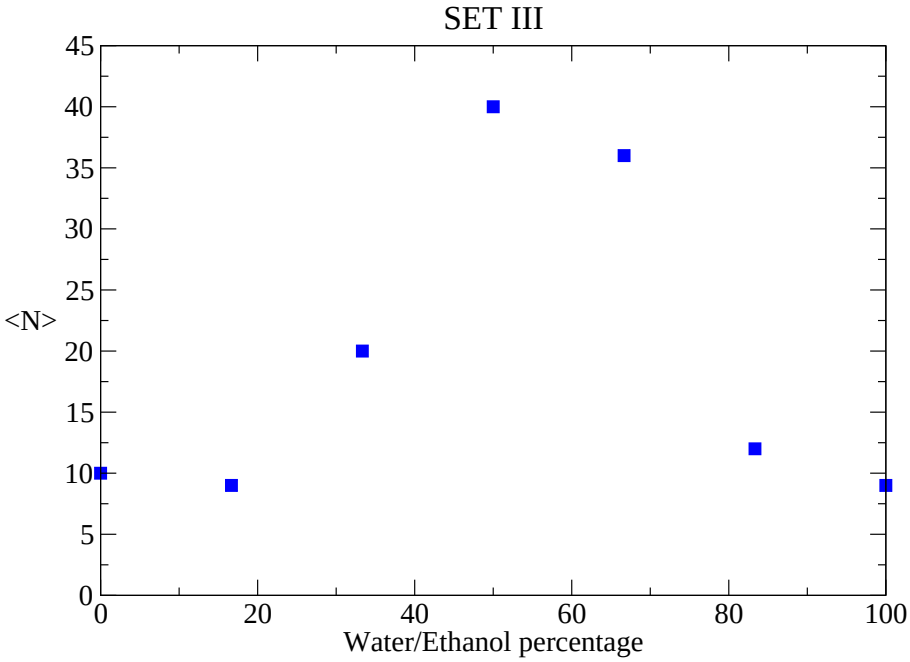

Figure 2.10: Average size of domain of the top layer ($< N >$) vs. water/ethanol percentage. Set 3: samples 3.A to 3.G

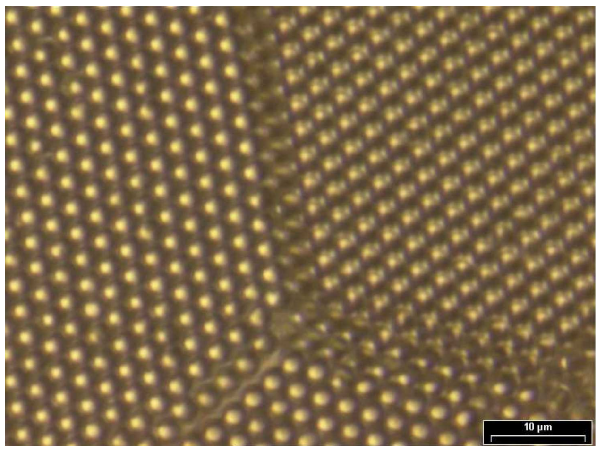

Figure 2.11: Detail of a crack found in sample 1.170.

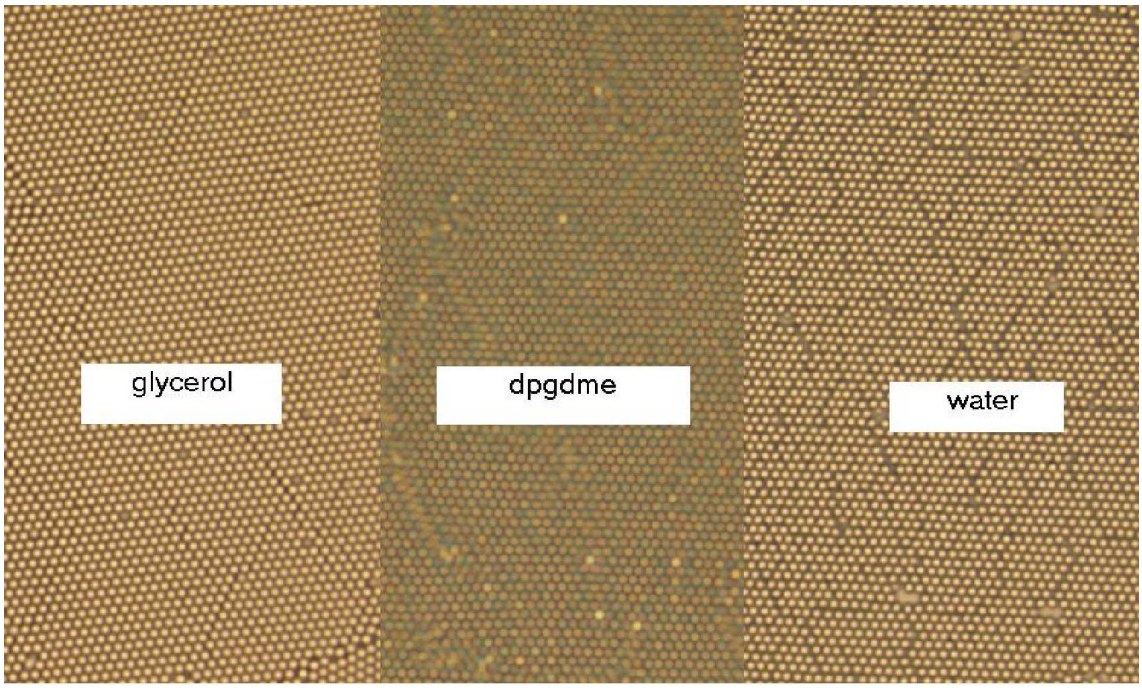

Figure 2.12: Optical micrography comparing the presence of crack in samples 7.W, 7.G and 7.DPGDME.

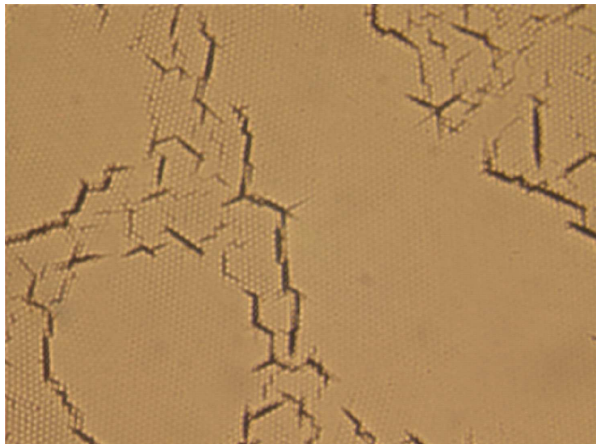

Figure 2.13: Optical micrography of sample 7.NMP.

Results from set 9 reveal that the best interval of concentration for the co–solvent is between 0.5 and 1% (w/V). At lower concentrations no effect takes place. At higher ones, particles are partly solved in the co–solvent and a film is observed. Polystyrene is not soluble in none of these co–solvents at the starting concentration, but the concentration of the co–solvent grows at the same time as the solvent evaporates. Because of that, particles can be finally solved in case of using too much co–solvent.

By using a co–solvent in the dispersion, the refraction index of the colloidal crystal changes, because a wet colloidal crystal is obtained. Wet colloidal crystals are more transparent than dry ones. Using glycerol as the co–solvent makes the material still more transparent.

Particle size

The particle size is the only different parameter between the last series of set 1, and sets 8 and 10 and set 11. In the first case it is 1.4 μm, in the second and the third 2.8 μm and in the last one 1 μm. When we measured the ordered area in the ordinary bidimensional units of (square μm, for instance) it was observed, as it can be expected, that the bigger particle size the higher size of domain. But when non–dimensional units (number of particles) are used, it is demonstrated that the maximum size of the domain does not depend of the particle size. Temperature, solvent and concentration should be optimized in order to prepare the structures with the maximum order. This maximum size of domain is the same for every particle size.

In figure 2.14 are represented the maximum size of domain, in non–dimensional units, for arrays prepared from particles of different sizes.

In figure 2.15 we compare micrographs of 1.4 μm and 2.8 μm arrays, made with 10 and 20 increases respectively.

Preparing the colloidal crystal in a mixture of water and heavy water (density matching) slows down the rate of sedimentation, which allows to work at lower temperatures to obtain better structures. For small particles it is possible to prepare high–quality colloidal crystal in water at low and high temperatures, but with large particles, such the ones of 2.8 μm, it is better to use heavy water at low temperatures in order to avoid a sedimentation of the particles too fast, which would avoid the self–assembly of the colloids (see figure 2.14)

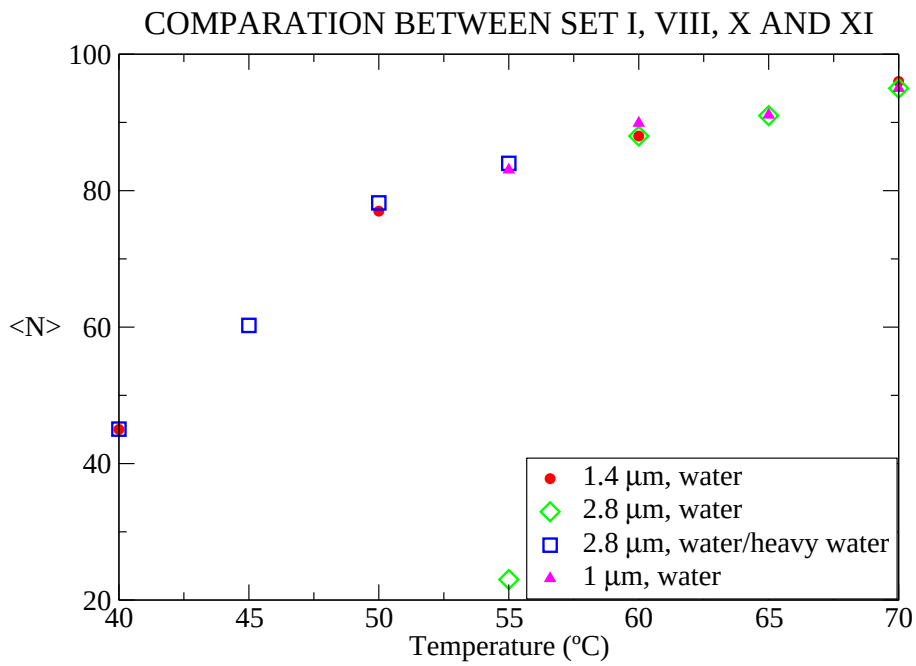

Figure 2.14: Non–dimensional size of domain vs. hydrodynamic diameter of the colloidal particle. Circle: samples 1.140 to 1.170, diamonds: samples 8.H65 to 8.H70, squares: samples 10.140 to 10.155 and triangles: samples 11.160 to 10.170.

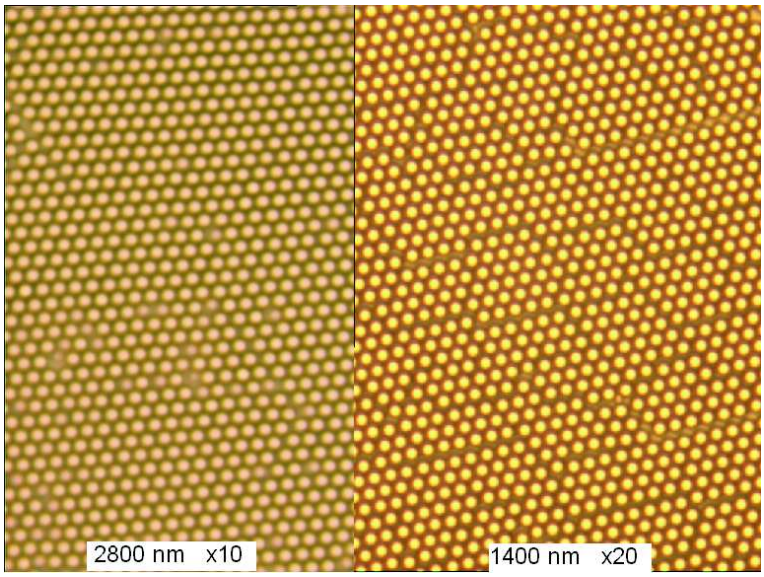

Figure 2.15: Hexagonally arrays of 1.4 and 2.8 μm particles., samples 1.170 and 8.170 respectively.

Optical properties

The structures were characterized by optical and diffraction microscopy and by transmission and angle dependent reflectance spectroscopy in vis–NIR–IR.

1. Normal incidence transmission spectroscopy

   Figure 2.16 shows the changes in the optical transmission spectra of films of two different thickness made using equal sized particles (1 μm diameter, determined by optical microscopy).

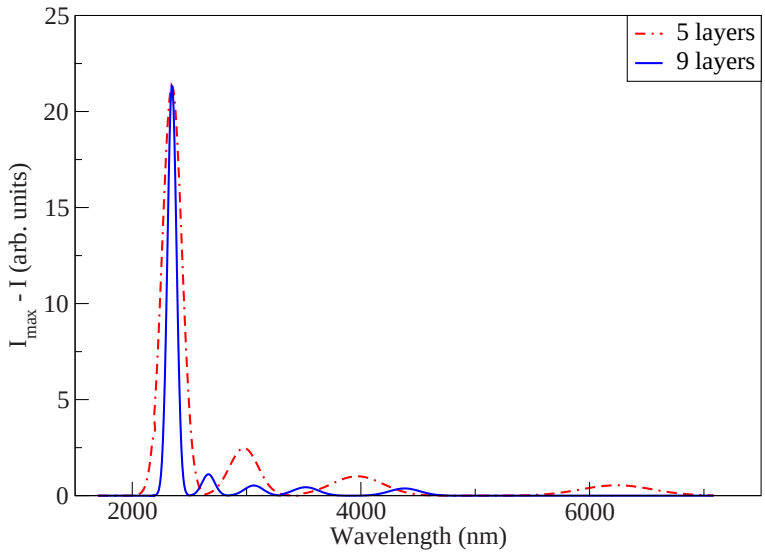

Figure 2.16: Normal incidence transmission spectra (optical density) of samples of 1 μm diameter with increasing film thickness. (Samples 11.160 and 11.170)

For polystyrene fcc colloidal crystals, $\Psi = 0.74$, $n_{PS} = 1.59$, $n_{eff} = 1.44$ and $d_{111} = 816.5$ nm. Thus, the peak position predicted from equations 2.1 and 2.4 is 2351.52 nm (4252 cm^{-1}). As it can be seen in figure 2.16, the agreement of these theoretical values with the experimental data is quite good (experimental stop band at 2347.83 nm (4259 cm^{-1}).

Two notable features of the spectra of figure 2.16 were sharp peaks due to the Bragg diffraction of IR light from the ordered spheres and a background rising a shorter wavelength. Typically at the peak maximum only 10–20% of the incident light is transmitted. These curves has been scaled to a constant height and the rising background apparent in the data has been subtracted because for samples of a thickness of more than 3 μm, this background contributes at most 20% of the rejection of light at the peak maximum. The intensity of the diffracted peak increases approximately linearly with the number of layers. Also, the peak width narrow as sample thickness is increased. Finally, Fabry–Perot fringes become smaller and more closely spaced in thicker samples. Because of that, determining the thickness of a sample by this method is good enough with samples up to 8 μm, depending on particle size.

By optical microscopy, areas with 4 and areas with 5 layers were found in sample 11.160, and 7 to 9 layers in sample 11.170. When the fringe order, p, was plotted versus the weighted maxima peak position, a straight line was obtained (see figure 2.17 and equation 2.7).

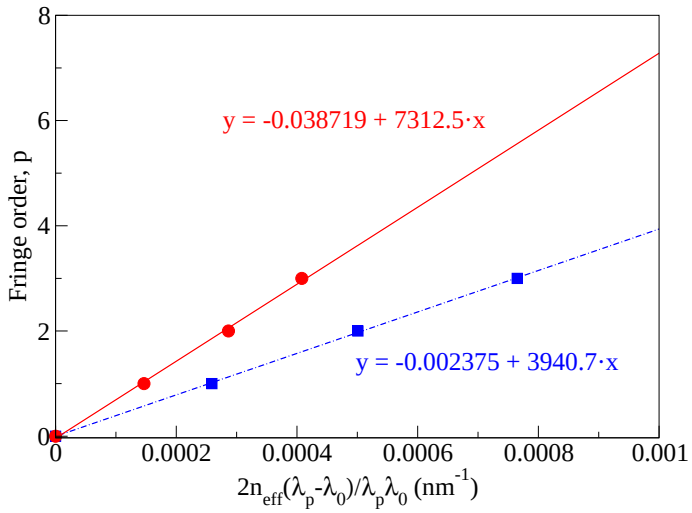

Figure 2.17: Fringe order, p, versus weighted maxima position, for samples with increasing thickness (Samples 11.160 and 11.170. 5 and 9 layers, respectively).

The thickness of the sample was obtained from the slope of the lines, 3940.7 and 7321.5 nm, respectively. The theoretical thickness for 5 layers in a fcc of 1000nm spheres, oriented with (1 1 1) planes on their surface is 4082 nm, and 7348.5 nm for 9 layers.

2. Angle dependent reflectance spectroscopy

   A 3D fcc lattice is confirmed by observation of well–developed (1 1 1) and higher order Bragg peaks and their angular dependence in reflectance spectroscopy.

   Figure 2.18 shows reflection spectra measured at different angles of incidence (10, 20, 25, 30, 35, 40 and 50°) with the polarization perpendicular to the plane of incidence, for particles of 1 μm, 1.4 μm and 2.8 μm. The curves has been vertically offset for clarity. The first–order diffraction peak, related to the (1 1 1) crystallographic planes, is seen at wavenumbers ranging from 4300 cm^{-1} to 5000 cm^{-1}, for 1 μm particles; from 3100 cm^{-1} to 3600 cm^{-1}, for 1.4 μm particles; and from 1600 cm^{-1} to 1800 cm^{-1}, for 2.8 μm particles. It can be seen that the wavenumber of the first–order Bragg peak increases monotonously with the angle of incidence. Also can be observed that the intensity of the peak is larger at higher angles of incidence, because more light is reflected. Comparing all the figures, it can also be seen that the bigger lattice constant (corresponding to a bigger particle size), the smaller wavenumber. The spectra also show the second–order diffraction peaks, whose wavenumbers first increase and then decrease with the angle of incidence in the range of 5090–5250 cm^{-1}

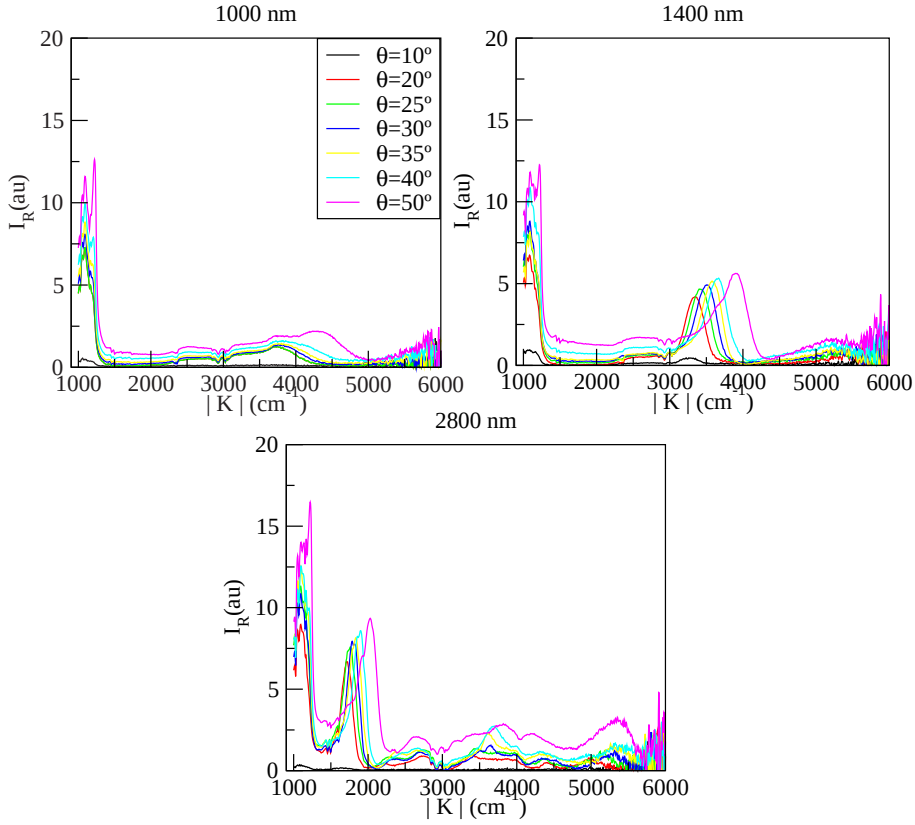

Figure 2.18: Reflection spectra at different angles of incidence for samples 11.160, 1.160 and 10.160 (1, 1.4 and 2.8 μm diameter, respectively.

and 2650–3570 cm^{-1} for 1.4 and 2.8 μm particles, respectively. And also a very intense peak at 1000 cm^{-1}, whose position is constant for every angle and particle size. While the second–order diffraction peaks are related to other unidentified crystallographic planes, the intense peak at 1000 cm^{-1} is not related to any crystallographic plane but to the reflection of the material (PS) itself. Only the peaks caused by the reflection of crystallographic planes depend on the particle size. Because of that, the last peak always appears at the same position (1000 cm^{-1}).

It is important to notice that, for these large particles (> 1 μm) the Bragg peak at 50° presents a smaller slope, which is not observed in small particles. Their cause is being studied.

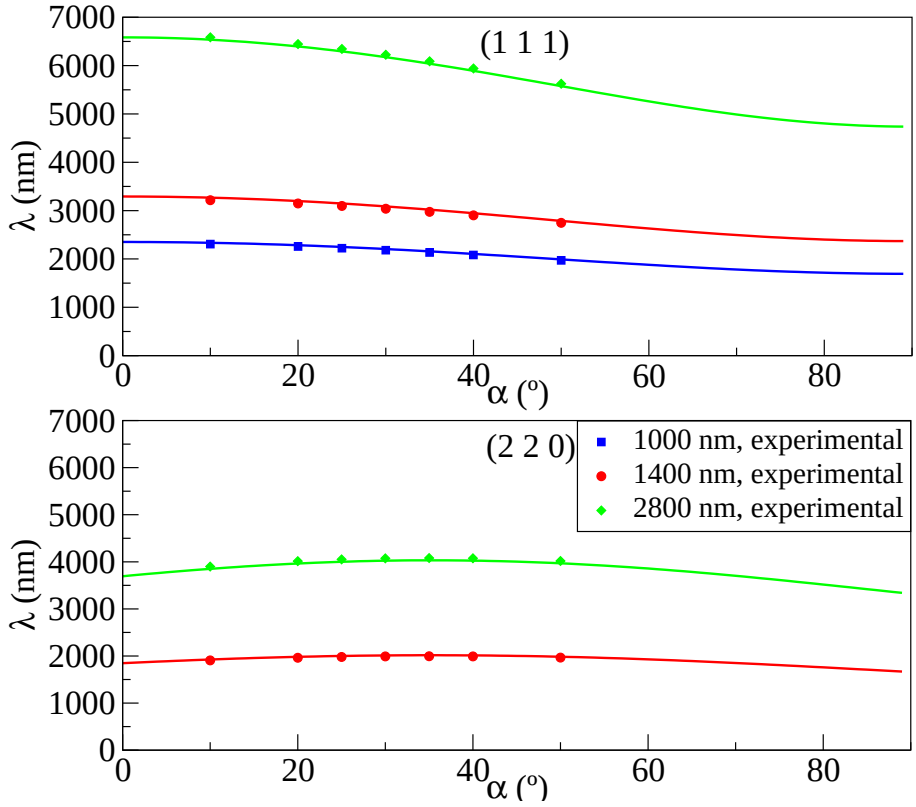

Figure 2.19: Non–linear fit of Bragg equation, for the fist and second Bragg peaks. Theoretical and experimental values.

We have extracted from the experimental data of the first Bragg peak, the dependence of the peak intensity wavelength on the incidence angle and fitted to the equation 2.9. The non–linear fit of the first peak yields to determine the sphere diameters and the effective refractive index of the samples. The non–linear fit of the second peak yields to determine the angle α, which allows to know which crystallographic plane is responsible for this diffraction. These results are summarized in table 2.2.

Table 2.2: Parameters determined by a non-linear fit of Bragg equation

	1st peak			**2nd peak**		
	BMG–24	PS–34	BMG–60	BMG–24	PS–34	BMG–60
D (nm)	983.96	1368.83	2811.36	-	1378.42	2817.75
$\mathbf{n}_{eff}$	1.45	1.45	1.44	-	1.45	1.45
α	-	-	-	-	35.29	35.26

For an α of 35.26° and a d/D of 0.5, the (2 2 0) is the only crystallographic plane allowed by crystallographic rules. For an arrangement of 1 μm particles, the peak corresponding to (2 2 0) planes should appear between 7100 to 7300 cm^{-1}. This interval is out of the spectrometer range, where the spectrum presents a lot of noise. Because of that, no second–order diffraction peak was found for 1 μm particles.

As it can be see in figure 2.19, all the data are in good agreement with the expected values.

3. Optical diffraction

Hexagonal reflections were generally observed using optical microscope with Bertrand lens for well–ordered arrays, although cubic reflections are sometimes also observed. Diffraction patterns from some hexagonally and cubically ordered mono–, bi–, tri– and multilayers of 1.4 and 2.8 μm particles are shown in figures 2.20, 2.21, 2.22 and 2.23.

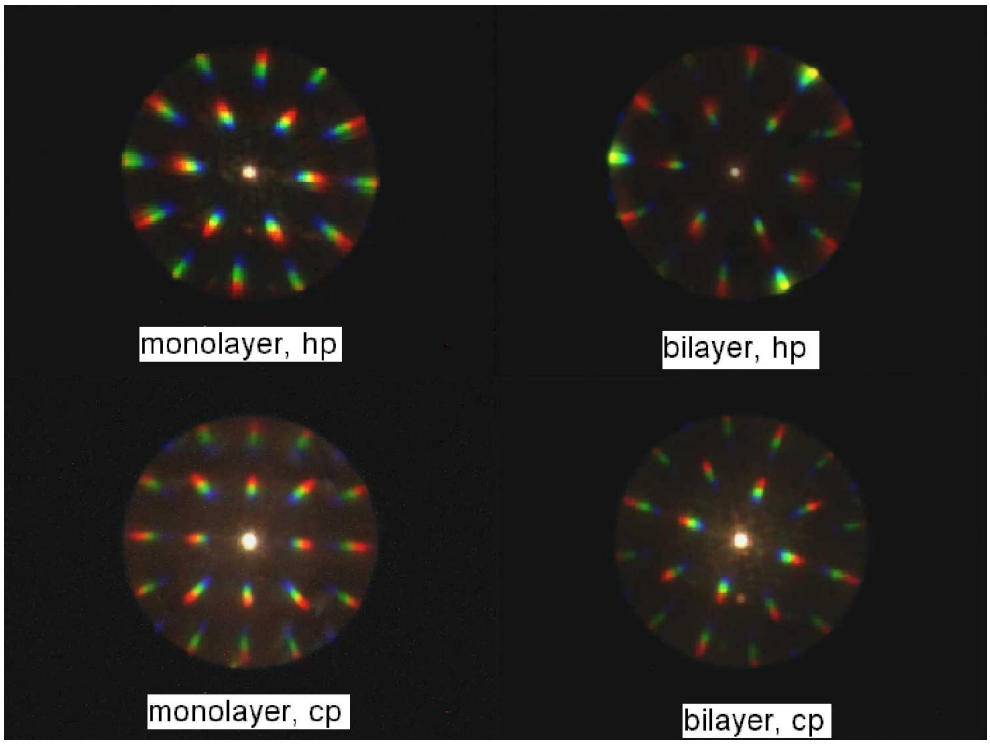

Figure 2.20: Diffraction patterns from some hexagonally and cubically ordered mono– and bi–layers of 1.4 μm particles. Images obtained from sample 1.160.

It is interesting to notice that, the bigger lattice constant (that corresponds to a bigger size of particle), the more orders of diffraction can be observed. This is very interesting to study complicated patterns, such as the ones generated by arrangements with more than two or three layers.

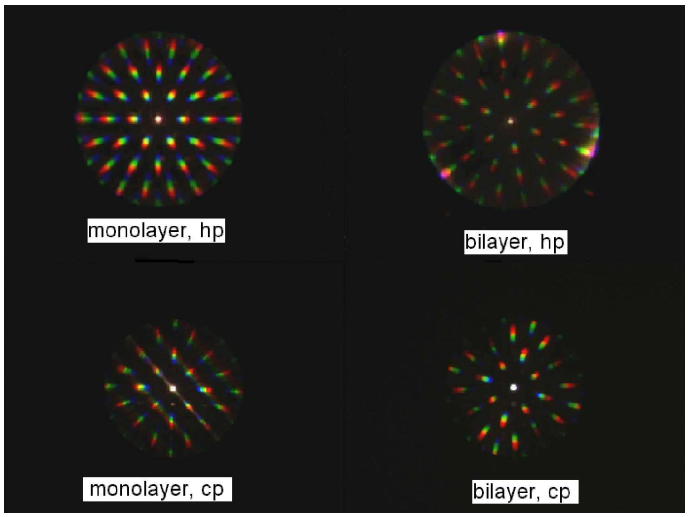

Figure 2.21: Diffraction patterns from some hexagonally and cubically ordered mono– and bi–layers of 2.8 μm particles. Images obtained from sample 11.170.

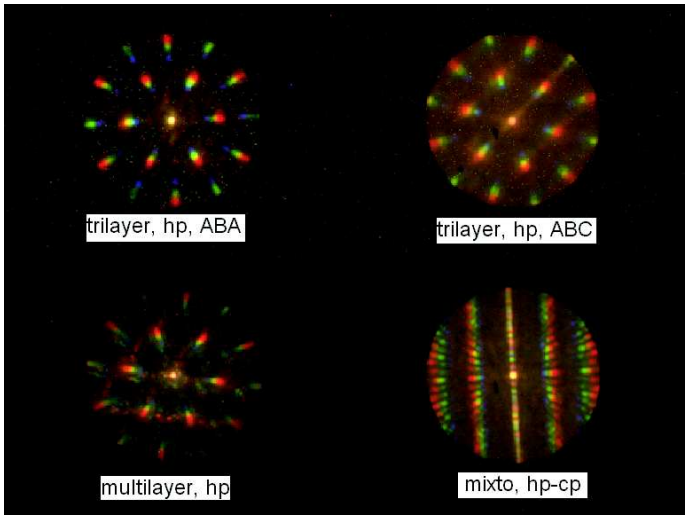

Figure 2.22: Diffraction patterns from some hexagonally hexagonally ordered multi–layers of 1.4 μm particles. Images obtained from samples 1.160 (trilayer ABA and ABC) and 1.170 (multilayer and mixed)

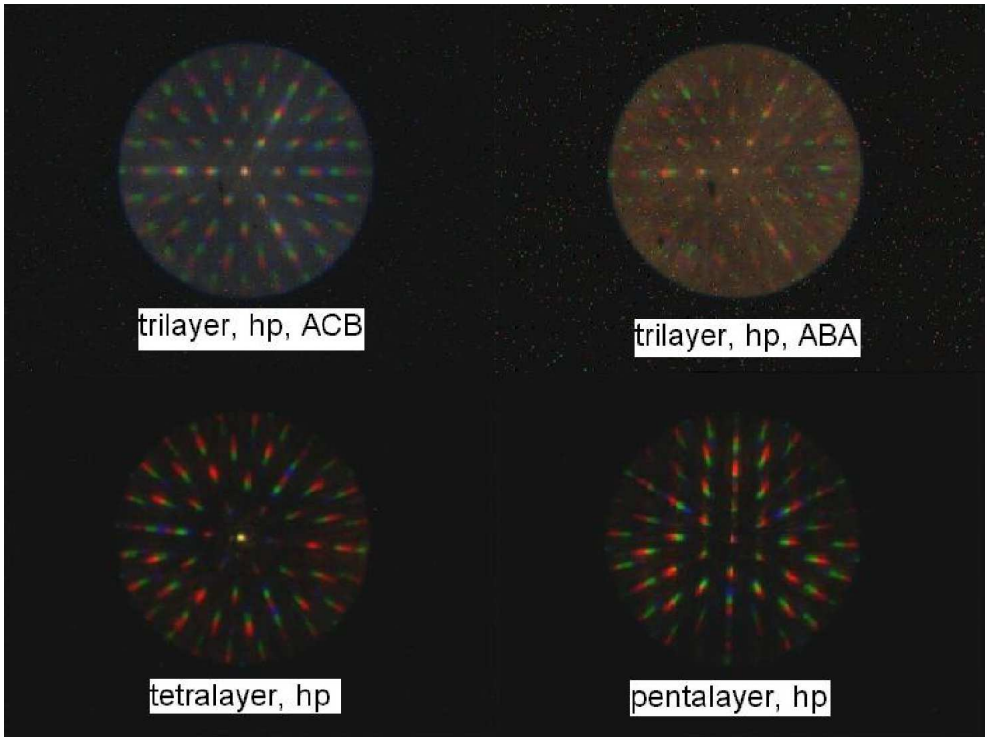

Figure 2.23: Diffraction patterns from some hexagonally hexagonally ordered multi–layers of 2.8 μm particles. Images obtained from sample 11.170.

The R(595 nm)–, G(532 nm)–, B(463 nm)–intensity profiles[1] in (1 0)–direction from some hexagonally and cubically ordered mono–, bi– and tri–layers of 1.4 and 2.8 μm particles are shown in figures 2.24, 2.25 and 2.26.

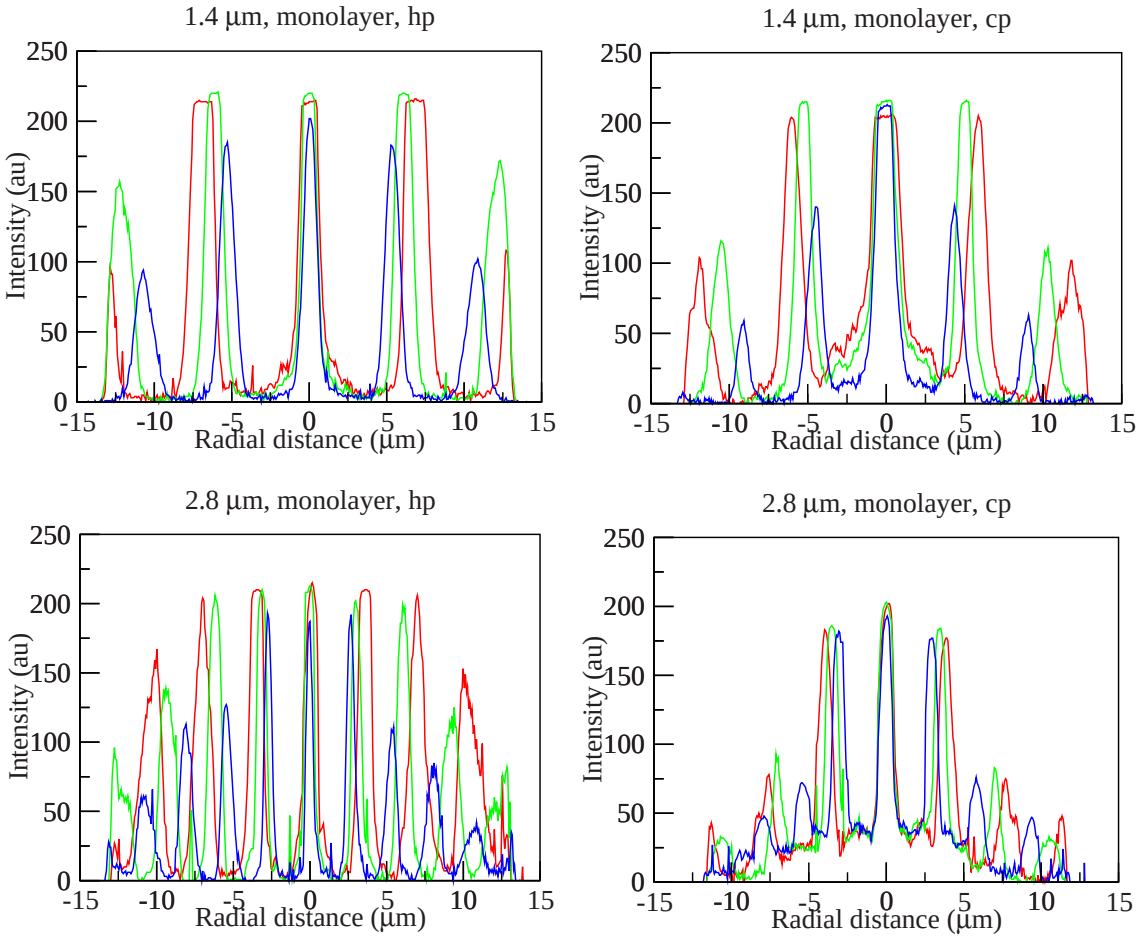

Figure 2.24: RGB–Intensity profile from different monolayer arrangements of particles of 1.4 (sample 1.160) and 2.8 (sample 11.170) μm. (Diffraction in (1 0)–direction)

[1]The wavelength corresponding to the R, G and B channels of the CCD camera have been identified by the procedure described earlier.

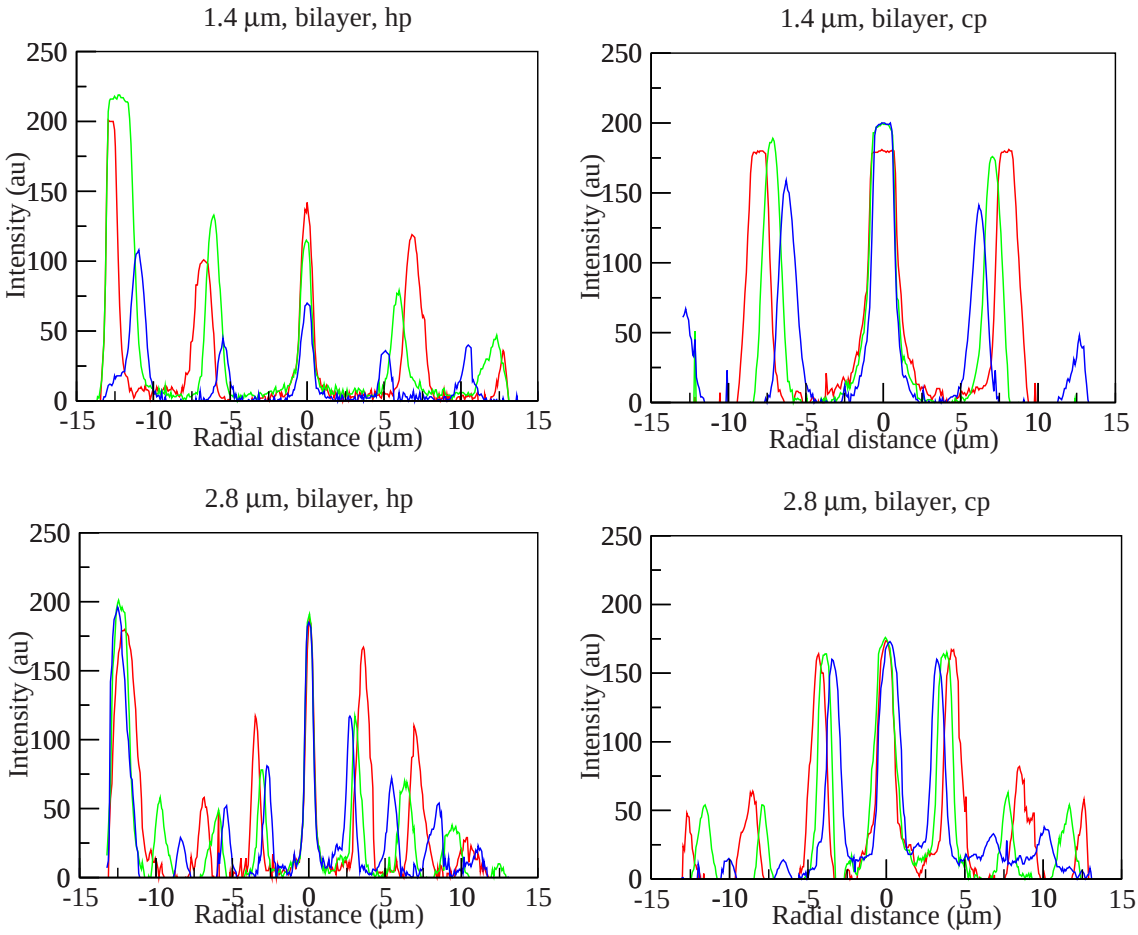

Figure 2.25: RGB–Intensity profile from different bilayer arrangements of particles of 1.4 (sample 1.160) and 2.8 μm (sample 11.170) (Diffraction in (1 0)–direction).

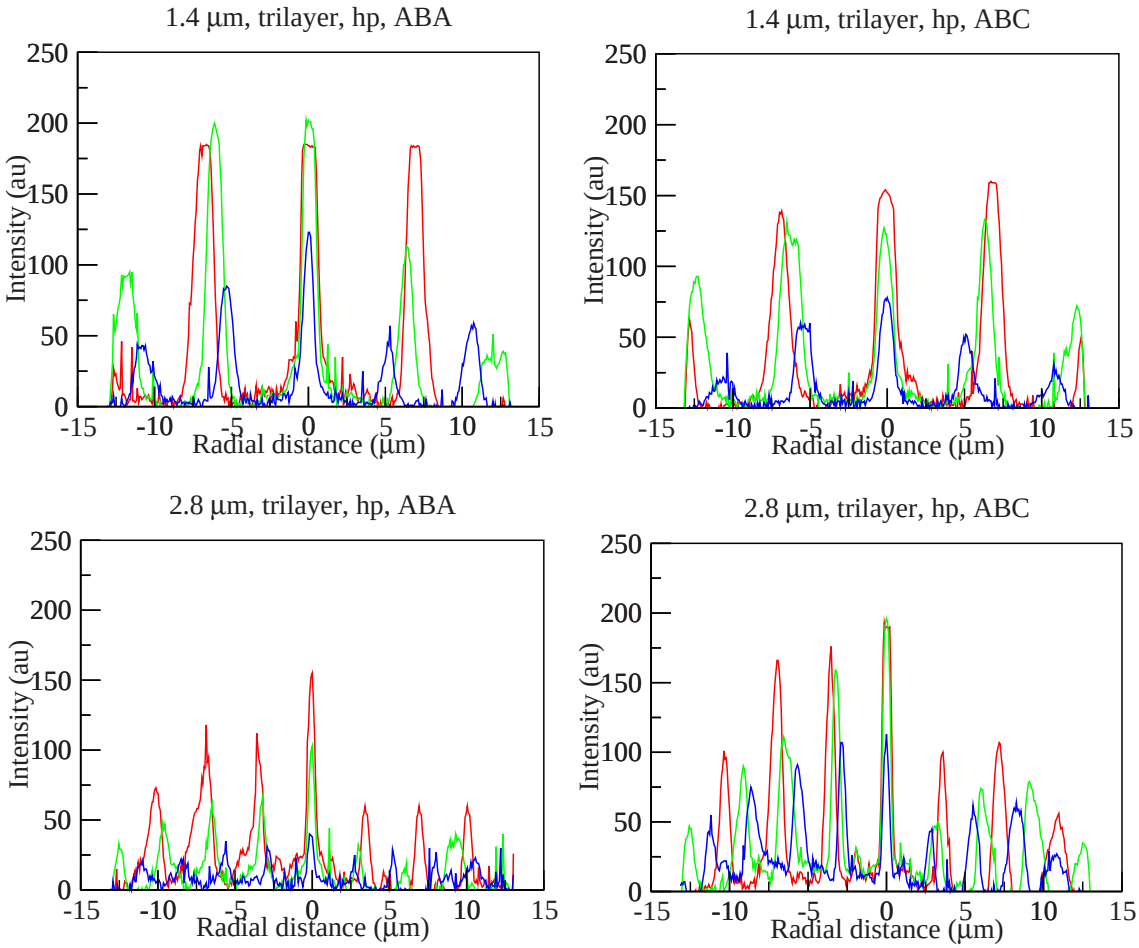

Figure 2.26: RGB–Intensity profile from different trilayer arrangements of particles of 1.4 (sample 1.160) and 2.8 μm (sample 11.170). (Diffraction in (1 0)–direction).

Nowadays, only 2D diffraction can be theoretically explained. Although the main direction of diffraction is the (1 0)–direction, it has been also recognized diffraction in the (1 1)– and (1 2)–direction. Hexagonal reflections are observed for hexagonal arrangements of particles, and cubic ones when particles present square symmetry.

From the multilayered particle arrays, a similar hexagonal or cubic diffraction pattern is observed in most cases with the difference that the light intensity in the central spot (zero order) is decreased compared with the first and higher diffraction orders and the color of the zero order is changed in accordance with color effects observed in the microscopic imaging of ordered particle layers. However, the positions of the intensity peaks were found to be independent of the number of layers and fit to a simple 2D diffraction (compare figures 2.24, 2.25 and 2.26). This seems to be in contradiction with spectroscopic and structural studies confirming the presence of fcc, possibly with a part of hcp, 3D crystal structure. This behavior can be explained according to Campbell et al. [64] by the diffraction dominated by coupling between the incident beam and the surface modes. The authors observed six first–order spots with 3 spots more intense than the others. The question of diffraction of the light on a 3D grating (analogue of von Laue X–ray experiment) constituting fcc, hcp or

rcp lattice is not clear yet. There is no contradiction, whether fcc–twinning takes place or not. According to Amos et al. [23], hexagonal reflections are observed for 2D hexagonal arrays and for rcp structures. For a twin–free fcc structure only three diffraction spots are expected (trigonal symmetry). Also in opinion of Cheng et al. [65], hexagonal spots correspond to rcp lattice and fcc lattice should lead to another diffraction pattern. On the contrary, according to Vlasov et al. [66], hexagonal reflections were observed for well ordered arrays of silica particles obtained by vertical deposition.

Interestingly enough, patterns from trilayered arrays were also observed. In these cases instead of six spots the light is diffracted predominantly in three directions with increasing intensities in the second and third diffraction orders (see again figures 2.22 and 2.23). In analogy to observations of Amos et al.[23] for shear aligned hard–sphere colloidal crystals, this effect could be interpreted as a result of single oriented fcc stacking sequences. Similar effects of trigonal light intensity distribution were also observed for relatively thick multilayers of particles, particularly when the sample transparency was increased by filling the voids of the array with a liquid (e.g. glycerol). Several types of diffraction patterns were recognized, which differ also in the orthoscopic image. These were assigned to the layer structure (ABA, ABC or random stacking).

Along the dominating hexagonal ordered domains tetragonal and intermediate structures were found. These could be assigned to the arrangement of (1 1 0) plane of the fcc lattice parallel to sample surface.

Each type of layer arrangement, which number increases with the number of layers (3, 4, 5, ... layers), generates a different and characteristic diffraction pattern. Because of that, diffraction analysis can be used to determine the crystalline structure and the stacking of a colloidal crystal.

Some systematic conclusions can be extracted from the experimental data:

1. Monolayer
   Predominantly hexagonal but in some cases also square packings were found.
   For hexagonal packing, the diffraction pattern shows six peaks.
   The central spot is very intense, and the intensity decreases with order.
   Diffraction in (1 0)–direction is more intense than the one in (1 1)–direction.
   "(1,2)-peaks" were also found.
   For square packing, the pattern present the same characteristics but with four peaks instead of six (peaks with the same distance to zero order).
   Patterns from 1.4 and 2.8 μm only differ in the number of orders, higher for larger particles.

2. Bilayer
   Both hexagonal and cubic packings were found.
   For hexagonal packing, diffraction patterns are hexagonal too.
   Not only the central spot is not very intense but also higher orders are more intense as the 1^{st} one.
   According to higher diffraction orders, 2^{nd} order for 1.4 μm particles and 3^{rd} order for 2.8 μ particles, the pattern seems to be trigonal.

Diffraction in (1 0)–direction is more intense than the one in (1 1)–direction
The diffraction pattern of cubic packing is similar for a monolayer or a bilayer, with slight differences: in the 1^{st} order, four peaks are more intense than the other four. At higher orders, diffraction in (1 1)–direction is more intense than the one in (1 0)–direction.
Patterns from 1.4 and 2.8 μm only differ in the number of orders, higher for larger particles. Their intensity profiles are very interesting and show more differences (see figure 2.25).

3. Trilayer
   Only hexagonal packings were found.
   Both ABA and ABC layer stackings were observed.
   Diffraction patterns present six peaks, but three of them are more intense than the others.
   The intensity of the spots is similar at every order apart from the zero one, which is not as intense as the others.
   Diffraction in (1 0)–direction is more intense than the one in (1 1)–direction
   For ABA structures, the central spot is more intense than for ABC structures.
   The color of the pattern is different in both cases (see 2.22 and 2.23).
   Patterns from 1.4 and 2.8 μm only differ in the number of orders, higher for large particles.

4. Tetralayer
   Only one "modification" of layer stackings was investigated here.
   Hexagonal pattern was observed in 1^{st} order, which is not intense.
   The intensity increases with order.
   At higher orders, the pattern changes from hexagonal to "double trigonal": three "blue" intense spots and other three "red" spots less intense.
   Diffraction in (1 1)–direction is as intense as in (1 0)–direction.

5. Pentalayer
   Hexagonal reflections were found in 1^{st} order, which is more intense than for a tetralayer.
   Intensity also increases with order.
   The central spot is red.
   The pattern present the "double trigonal" appearance at higher orders.
   Diffraction in (1 1)–direction is as intense as in (1 0)–direction

6. Multilayer
   Pattern present similar appearance as for a monolayer, but the central spot is less intense.
   1^{st} order very intense, but less than in a mono or bilayer
   Diffraction in (1 1)–direction is as intense as in (1 0)–direction

2.2 Sedimentation

Although the principle responsible for self–assembly is the balance between solvent evaporation rate and particle sedimentation for both vertical deposition and sedimentation, this balance is different in these two processes, due to the geometry of the system. While vertical deposition involves to place a nearly vertical substrate in the suspension of colloidal spheres, sedimentation places the substrate horizontally, on the dispersion.(compare figures 2.1 and 2.27). In this second process, the relative humidity in the system plays also an important role.

2.2.1 Experimental section

Substrates and material

Hydrophobic PS latex particles with a narrow size distribution and a diameter of 1.4 μm (PS–34) were prepared by an emulsifier–free, aqueous radical polymerization [34; 35; 36].
Aqueous ammonium hydroxide (25% V/V) was provided by PANREAC, hydrogen peroxide (30% V/V) by Merk and KNO_3 (pure, >99%) by Merk .
Ultra pure water, 1 μ/cm conductivity, was used from a Mili–Q water system.
Comercial ultra sounds cleaner for optical material, OPTIC II SUPER, is provided by Technological.
10x26 mm glass slides provided by Roth Karlsruhe were used as substrates.

Method

Latex is prepared in the same way as for vertical deposition: all dispersions were diluted with ultra pure water to a concentration of 0.1–1%(w/V) and deeply mixed by applying ultrasounds 10 minutes at half power and room temperature, before use. When the latex was not recently synthesized, it was previously filtered using a 8 μm filter. When glycerol was used as a co–solvent, first a solution 1:1 glycerol:water was prepared, in order to decrease glycerol viscosity to make their manipulation easier. 20 μm of this dilution was added for each ml of latex.

However, substrates (glass slides of 12 mm x 25 mm, thickness 1mm) were perfectly cleaned in two different ways. The first method is the same hydrophilization than for vertical deposition. After this process, the substrates become very hydrophilic. The second one consists on putting them inside a glass with a commercial cleaner (OPTIC SUPER II) and applying ultrasound for 5 minutes, at 50°C and maximum power. After that, rinsing three times with desionized water and once more with ultra pure water. That makes the substrates very hydrophobic.

Samples were prepared in the sedimentation cell shown in 2.27.

In a representative procedure, the cell was filled with a saturated solution of KNO_3. Substrates were placed on the porta samples and 10 μm of latex is put on the substrates. After that the cell is covered with a glass slide.

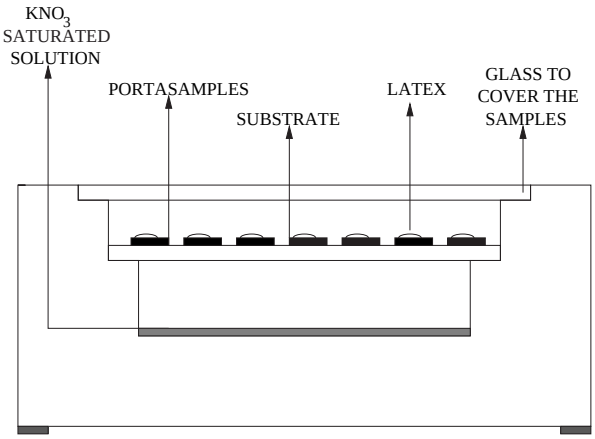

Figure 2.27: Sedimentation cell sketch.

Parameters of control

There are some parameters which allow to control the solvent evaporation rate.

1. Solvent
   Samples in ultra pure water and samples in ultra pure water with glycerol as co–solvent were prepared.

2. Temperature
   Samples were prepared at several temperatures, from room temperature until 50°C

Another parameters allow to regulate the sedimentation of particles. These are:

1. Particle size
   Particles of 1.4 were studied

2. PS concentration
   The range of concentration studied was from 0.1 to 1% PS (w/V)

3. Substrate
   Cleaning methods of hydrophilization and commercial cleaner were compared.

Proposed experiments

In table 2.3 there are summarized the samples prepared by sedimentation.

Table 2.3: Samples prepared by sedimentation.

Set	Substrate	Particle size (μm)	[PS] (% w/V)	Temperature (°C)	Solvent	Sample
4	hydrophilized glass hydrophobized glass[5]	1.4	0.1–1	50	water	4.H01–4.H1 4.C01–4.C1
5	hydrophilized glass	1.4	0.1	50	water co–solvent (glycerol) (0/1%)	5.H01–5.H1 5.HG01–5.HG1 5.C01–5.C1 5.CG01–5.CG1
6	hydrophilized glass hydrophobized glass	1.4	0.1–1	25	water co–solvent (glycerol) (0/1%)	6.H01–6H1 6.HG01–6.HG1 6.C01–6.C1 6.CG01–6.CG1

2.2.2 Characterization

Optical microscopy and single domain diffraction of white light were made to study the size of domain, the crystalline structure and the optical properties of the samples.

2.2.3 Results

Temperature

The higher temperature, the bigger rate of evaporation. As they are large particles, sediment very quickly and self–assembly takes no place at high temperatures. Besides, for temperatures higher than the room temperature, very small domains were obtained. It has been proved that at high temperatures sedimentation is not a good method to prepare colloidal crystals based on large latex particles.

The size of domain achieved at room temperature is of the same order as the one obtained by vertical deposition at 60–70°. Therefore, a disadvantage of sedimentation compared to vertical deposition is that the size of domain can not be improved by changing the temperature, while in vertical deposition grows with it.

PS concentration

The higher PS concentration, the higher size of domain. For PS concentration smaller than 1%(w/V), no monolayer was prepared, only small groups of particles were observed. Thus, the behavior is similar to the one explained for vertical deposition.

Solvent

In the results of set 6, it was shown that using glycerol as a co–solvent increases the size of domain in the final ordered arrays, not only when colloidal crystallization is made by vertical deposition but also when it is done by sedimentation. In this last process, the size of domain is increased up to 5 times (see figure 2.28).

[5]H for the hydrophilized and C for the hydrophobized substrates.

Substrate

Figure 2.28 shows that higher size of domain were obtained using the hydrophilic substrates (prepared by hydrophilization), than the hydrophobic ones obtained by cleaning with the commercial cleaner. These results confirm what was commented for vertical deposition.

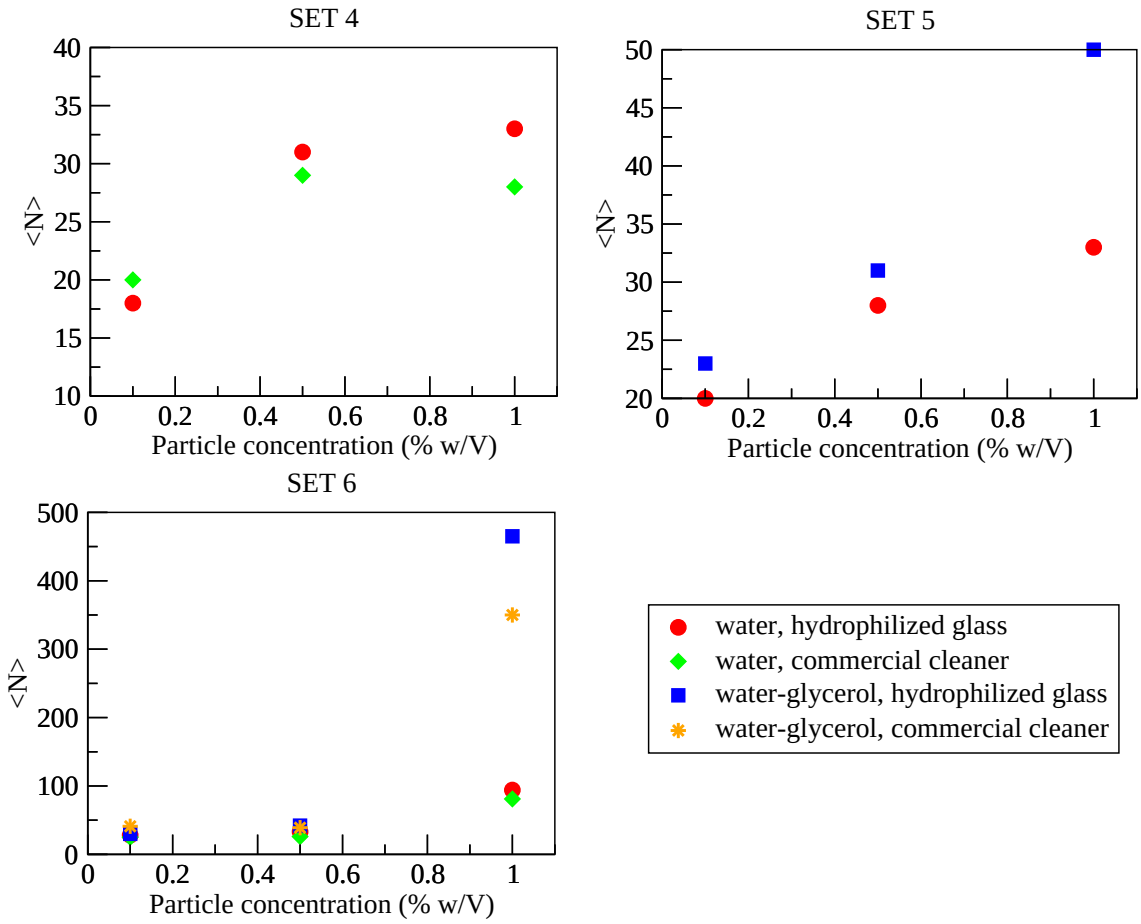

Figure 2.28: Size of domain of samples prepared in sets 4, 5 and 6.

All the samples present the same hexagonally and cubically ordered arrangements of particles as the ones explained for samples prepared by vertical deposition.

Chapter 3

Conclusions

Hydrophobic and smooth (BMG–7), hydrophobic and rough (BMG–60) and hydrophilic and smooth colloidal particles (BMG–24) of 1.4 and 2.8 μm, were synthesized by modified emulsion and dispersion polymerization techniques based in styrene and acrylate monomers

After synthesis, the latex should be cleaned and purified by dialysis and ultrafiltration, in order to prepare high monodisperse latexes (PI<5%).

The polymeric colloidal particles can be stabilized in water dispersion by electrostatic repulsion (BMG–7), steric impediment (BMG–60) or electrosterical interactions (BMG–24).

A systematical study of the electrokinetic properties of the three types of particles through titration, Dynamic Light Scattering and zeta–potential measurements, reveals that the behavior of both BMG–7 and BMG–24 particles depends on their surface charge density and can be properly explained by the DVLO theory. However, BMG–60 particles depends more on the configuration of their lateral chains and can not be properly controlled.

As large latex particles electrostatically stabilized present problems of coalescence in the first steps of the vertical deposition and the ones sterically stabilized can not be properly controlled during the process, it is adequate to stabilize the latex both by electrostatic repulsion and by steric repulsion (core–shell particles, BMG–24).

2D and 3D colloidal crystals up to 4 cm^2 in size (with monocrystalline domains up to 10^4 μm) and up to 50 layers are prepared by vertical deposition and by sedimentation. These domains present preferably stackings of hexagonally close packed particle layers resulting in fcc, hcp and rhcp crystalline structures.

The size of the monocrystalline domains is determined by optimizing the main parameters of control. Although this optimization depends on the size and nature of the colloidal particles, once the system is optimized, the non–dimensional maximum size of does not depend on particle size.

The temperature, substrate, particle concentration and medium of deposition are the most important parameters of control. Thus:

- The higher the temperature (from 40 to 70°), the higher order in the structures.
- Hydrophilized glass slides are the best substrates to do the vertical deposition of large polystyrene colloidal particles.
- The lower particle concentration (from 0.1 to 1 % w/V), the higher size of domain.
- Colloidal crystallization of 1.4 μm particles is improved in mixtures water/ethanol about 50% V/V, meanwhile colloidal crystallization of 2.8 μm particles is improved in mixtures water/heavy water 50% V/V.

Cracks are formed after colloidal crystallization, during the drying stage. However, the drying stage can be avoided by adding co–solvents to the medium of deposition, therefor reducing the number of cracks.

The best concentration for the co–solvents are 1% V/V.

Glycerol and dipropylenglycol–dimethylether are the best co–solvents in the self–assembly of polystyrene colloidal particles.

Optical micrographs reveal that the samples are oriented with their (1 1 1) planes parallel to the substrate.

Optical microscopy with Bertrand lens enables the investigation of single domain diffraction patterns (diffraction of white light) of large particles (>1 μm). Although the main direction of diffraction was the (1 0)–direction, sometimes the (1 1)– and (1 2)–directions were also observed.

The higher size of particle, the more orders of diffraction are observed.

Hexagonal reflections were generally observed, although cubic patterns were sometimes determined too.

A spectral and spatial redistribution of light was observed in the diffraction pattern when increasing the number of layers: the light intensity of the central spot (zero order) is decreased compared with the first and higher diffraction orders, and its color is changed in accordance with color effects observed in the micrographs of ordered particle layers. However, the positions of the diffraction peaks were found to be independent of the number of layers and fit to a simple 2D diffraction.

Well developed stop–bands were detected in the spectral region between 3000 and 6000 nm, depending on the particle size.

Particle size and effective refraction index of the sample as well as the crystallographic planes involved were determined from reflection spectroscopy experiments, by a non-linear fit of the dependence of the peak wavelength on the incidence angle to the Bragg equation (1 1 1) and (2 2 0) planes were found.

The thickness of the samples was accurately determined from transmission spectroscopy measures, by analyzing the position of the Fabry–Perot fringes.

Bibliography

[1] E. Yablonovitch, Phys. Rev. Lett., **58**, 2059, 1987.

[2] S. John, Phys. Rev. Lett., **58**, 2486, 1987.

[3] W.B. Russel, D.A. Saville and W.R. Schowalter, "Colloidal dispersions", Cambridge University Press, 2^{nd} ed., Cambridge, 1991.

[4] D.F. Evans and H. Wennerstrom, "The colloidal domain: where physics, chemistry, biology and technology meet", Wiley-VHC, 2^{nd} ed., New York, 1999.

[5] J.W. Goodwin, "Colloids and interfaces with surfactants and polymers: and introduction", Wiley and Sons, Chichester, 2004.

[6] R.W. Jones, "Fundamental principles of sol-gel technology", Brookfield, 1^{st} ed., England, 1989.

[7] R.B. Seymour and C.E. Carraher Jr., "Introducción a la química de los polímeros", Ed. Reverté, 3^{rd} ed., Barcelona, 1998.

[8] M.P. Stevens, "Polymer Chemistry. An introduction.", Oxford University Press, 3^{rd} ed., New York, 1999.

[9] O. Somorin, Proccedings of the 2^{nd} International Conference on Chitin and Chitosan. The Japanese Society of Chitin and Chitosan, Tottori, 1982.

[10] W.H. Carothers, J. Amer. Chem. Soc., **51**, 2548, 1928.

[11] D. Brawn, H. Cherdron and H. Ritter, "Polymer Synthesis: Theory and Practice", Springer, 3^{rd} ed., Heidelberg, 2001.

[12] H. Freundlich, "Colloid and capillarity chemistry", Ed. Methuen, London, 1926.

[13] H.R. Kruyt, "Collid Science', Volume I', Ed. Elsevier, Amsterdan, 1952.

[14] R.J. Hunter, "Foundations of colloid science",Volume I, Clarendon Press, 2^{nd} ed., Oxford, 1991.

[15] A. Herzog, C.A. Paula, M.E. Darbello, F. Gallembeck, Colloids and Surfaces A, **144**, 207, 1998.

[16] F. Kopnov, V. Lirtsman, D. Davidov, Synthetic Metals, **137**, 993, 2003.

[17] E.W. Seelig, B. Tang, A. Yamilov, H. Cao, R.P.H. Chang, Materials Chemistry and Physics, **80**, 257, 2003.

[18] K.S. Mayya, M. Sastry, Langmuir, **15**, 1902, 1995.

[19] A. Stein, R.C. Schroden, Current Opinion in Solid State and Material Science, **5**, 553, 2001.

[20] L.M. Goldenberg, J. Wagner, J. Stumpe, B.R. Paulke, E. Görnitz, Materials Science and Engineering, **22**, 405, 2002.

[21] L.M. Goldenberg, J. Wagner, J. Stumpe, B.R. Paulke, E. Görnitz, Langmuir, **1**18, 3319, 2002.

[22] P. Nozar, C. Dionigi, A. Migliori, G. Calestani, L. Cademartiri, Synthetic Metals, **139**, 667, 2003.

[23] R.M. Amos, J.G. Rarity, P.R. Tapster, T.J. Shepherd, Physical Review E, **61**, 2959, 2000.

[24] O. Vickreva, O. Kalinina, E. Kumacheva, Advanced Materials, **12**, 110, 2000.

[25] M. Yoldi, W. González–Viñas, R. Sirera and C. Arcos, Proceedings of 2004 6^{th} International Conference on Transparent Optical Networks (edited by Marian Marciniak) volume 1, 330.

[26] V.J. Sanders, Nature, **24**, 1151, 1964.

[27] V.J. Sanders, Acta Crystallogr., **24**, 427, 1968.

[28] L.V. Woodcock, Nature, **385**, 141, 1997.

[29] P.G. Bolhuis, D. Frenkel, S.-C. Mau and D.A. Huse, Nature, **388**, 236, 1997.

[30] S.-C. Mau and D.A. Huse, Phys. Rev. E, **59**, 4396, 1999.

[31] Y.A. Vlasov, V.N. Astratov, A.V. Barishev, A.A. Kaplyanskii, O.Z. Karimov and M.F. Limonov, Phys. Rev. E, **61**, 5784, 2000.

[32] D.J. Norris, E.G. Arlinghaus, L. Meng, L. Heiny and L.E. Scriven, Adv. Materials, **16**, 1393, 2004.

[33] Q. Wang, S. Fu, T. Yu, Prog. Polym. Sci., **19**, 703, 1994.

[34] A. Kotera, F. Furusawa and Y. Takeda, Kolloid-Z.Z. Polym., **239**, 677, 1970.

[35] J.W. Goodwin, J. Hearn, C.-C. Ho and R. Ottewill, Colloid Polym. Sci., **252**, 464, 1974.

[36] B.-R. Paulke, P.-M. Möglich, E. Knippel, A. Budde, R. Nitzsche and R.H. Müller, Langmuir, **11**, 70, 1995.

[47] Y.Y. Lu, M.S. El-Aasser and J.W. Vanderhoff, J. Polym. Sci., B, Polym. Phys. **26**, 1187, 1988.

[38] K.S. Schmitz, "An Itroduction to Dynamic Light Scattering by Macromolecules", Academic Press, Inc., San Diego, 1990.

[39] http://www.physics.uoguelph.ca/GBLL/theory.html

[40] http://www.zeta-meter.com/redchile.pdf

[41] A.W. Adamson and A.P. Gast, "Physical Chemistry of Surfaces"6^{th} ed., John Wiley & Sons, Inc., Canada, 1997.

[42] L.A. Dissado et al., J. Phys. D: Appl. Phys., **22**, 713, 1989.

[43] A.S. Dimitrov and K. Nagayama, Langmuir, **12**, 1303, 1996.

[44] P. Jiang, J.F. Bertone, K.S. Hwang and V.L. Colvin, Chem. Mater., **11**, 2132, 1999.

[45] P. Jiang, K.S. Hwang, D.M. Mitternan, J. F. Bertore, V.L. Colvin, Am. Chem. Soc., **121**, 11630, 1999.

[46] Y.A. Vlasol, X.-Z. Sturm and D.J. Norris, Nature, **414**, 289, 2001.

[47] Y.Y. Lu, M.S. El-Aasser, J.W.J. Vanderhoff, Polym. Sci., Part B: Polym. Phys., **26**, 1187, 1988.

[48] J.M. Jethmalani and W.T. Ford, Chem. Mater., **8**, 2138, 1996.

[49] J.M. Jethmalani, H.B. Sunkara, W.T. Ford, S.L. Willoughby and B.J. Ackerson, Langmuir, **13**, 2633, 1997.

[50] W.L. Vos, R. Sprik, A. van Blaaderen, A. Imhof, A. Lagendijk and G.H. Wegdam, Phys. Rev. B, **53**, 16231, 1996.

[51] Y. Monovoukas, G.G. Fuller and A.P. Gast, J. Chem. Phys., **93**, 824, 1990.

[52] P.A. Rundquist, P. Photinos, S. Jagannathan and S.A. Asher, J. Chem. Phys., **91**, 4932, 1989.

[53] H.B. Sunkara, J.M. Jethmalani and W.T. Ford, "Hybrid Organic-Inorganic Composites", J.E. Mark, C.Y.-C. Lee and P.A. Bianconi, Ed.; American Chemical Society: Washington, DC, Vol. 585, p 181, 1995.

[54] D.M. Mittleman, J.F. Bertone, P. Jiang, K.S. Hwang and V.L. Colvin, J. Chem. Phys., **111**, 345, 1999.

[55] L. Liu, P. Li and S.A. Asher, J. Am. Chem. Soc. , **19**, 2729, 1997.

[56] B.D. Cullity, "Elements of X-ray Diffraction", 2nd ed.; Addinson-Wesley Publishing Company, Inc.; Reading, MA, 1978.

[57] E. Hecht, Optics, 2nd ed.; Addinson-Wesley Publishing Company, MA, 1987.

[58] J.F. Bertone, P. Jiang, K.S. Hwang, D.M. Mittleman and V.L. Colvin, Phys. Rev. Lett., **83**, 300, 1999.

[59] N. Lauinger, M. Pinnow and E. Görnitz, J. Biol. Phys., **23**, 73, 1997.

[60] M. Srinivasrao, D. Collings, A. Philips and S. Patel, Science, **292**, 79, 2001.

[61] L.M. Goldenberg, J. Wagner, J. Stumpe, B.-R. Paulke and E. Görnitz, Physica E, **17**, 433, 2003.

[62] G.N. Ramachandran and S. Ramaseshan, "Handbuch der physik", S. Flüge, 25/1, Springer-Verlay, Berlin, 1961.

[63] G.S. Lazarov, N.D. Denkin, O.D. Velev, P.A. Kralchevsky and K. Nagayama, J. Chem. Soc. Faraday Trans., 90, **14**, 2007, 1994.

[64] M. Campbell, D.N. Sharp, M.T. Harrison, R.G. Denning, A.J. Turberfield, Nature, **404**, 53, 2000.

[65] Z. Cheng, W.R. Russel, P.M. Chaikin, Nature, **401**, 893, 1999.

[66] Y.A. Vlasov, X.-Z. Bo, J.-C. Sturm, D.J. Norris, Nature, **414**, 289, 2001.